

RESEARCH ARTICLE

Open Access



Physics Linkages Between Arterial Morphology, Pulse Wave Reflection and Peripheral Flow

Trevor Tucker^{1*}

Abstract

Background Previous physics-based analyses of arterial morphology in relation to pulsatile pressure and flow, with pulse wave reflection, focused on the large arteries and required assumptions about the relative thicknesses of arterial walls and the velocities of pulse waves in the arteries. A primary objective of this study was to analyze arterial morphology and pulse wave reflection, using physics-based wave propagation, which explicitly includes arterial stiffness, with potential autonomic flow regulation, for both large and small arteries.

Methods Pulse wave reflections that occur at arterial bifurcations, and their impact on macrocirculation and microcirculation pulse pressures and flows, are analyzed using the physics of wave propagation and impedance matching.

Results The optimum combinations of arterial dimensions and stiffnesses which minimize pulsatile reflections at arterial bifurcations are identified for both macrocirculation and microcirculation. The optimum ratio of arterial bifurcations' branch-to-trunk luminal areas is predicted to have a value of 1.26, (with corresponding optimum stiffnesses) based on the principle that autonomic flow regulation minimizes pulsatile reflections. This newly predicted value of area ratio compares favorably with the Murray Scaling Law value of 1.26. For an area ratio of 1.26, the optimum bifurcation stiffness ratio is predicted to have a value of 1.12 for bifurcations in the macrocirculation and a value of 0.89 in the microcirculation. The analysis predicts that minimal pulsatile reflections may occur for area ratios not equal to 1.26, when vasodilation adjusts arterial stiffness to compensate for non-optimal arterial area ratios. The analysis predicts that the capillaries have about one-tenth the stiffness of the aorta, and the capillary bed possesses about one thousand times more total luminal area than the aorta. The analysis predicts there are about thirty generations, aorta to capillaries, of arterial bifurcations in an arterial tree.

Conclusions The optimum arterial morphologies predicted by this physics-based analysis correspond to those observed in human vascular physiology. The contributions that arterial stiffnesses and dimensions make to optimal pulsatile flow are relevant to the development of pharmaceuticals related to autonomic vasodilation, to the development of optimally designed stents and to surgical procedures related to vascular modification.

Keywords Arterial bifurcation, Impedance, Stiffness gradient, Area ratio, Pulse wave velocity, Reflection coefficient, Target organ ischemia, Hypertension, Womersley, Murray's Law

1 Introduction

The human arterial system in youth is described [1] as being “beautifully designed for its role of receiving spurts of blood from the left ventricle and distributing this as steady flow through peripheral capillaries”. The arterial system develops from the embryonic stage, through

*Correspondence:

Trevor Tucker
trevor_tucker@yahoo.com

¹ T Tucker Inc, Ottawa, ON, Canada



youth, into a complex tree-like structure, consisting of arteries of diminishing size and compliance, extending from the large central arteries into the fine arterioles and capillaries. The arterial system's design includes various autonomic regulatory processes for homeostasis maintenance of blood pressure and flow throughout the vasculature. These processes mediate flow at both the large artery (macrocirculation) and small artery (microcirculation) levels of the vasculature. Such autonomic processes, include biochemical (i.e., the renin–angiotensin–aldosterone system), cellular (i.e., endothelial dependent vasodilation), neurovascular (i.e., baroreflex and neuro-glial-vascular) and physical (i.e., the physics of flow) processes. The biochemical, cellular, and neurovascular contributions to the linkages between pressure in the macrocirculation and flow in the microcirculation are generally qualitatively described [2–8]. In comparison, the physical contributions to such linkages may be quantitatively described through the application of the physics of fluid dynamics and wave propagation and impedance matching to vascular flow.

Although specific control algorithms that determine arterial morphology and regulate blood flow in target organ perfusion are currently unidentified, a recent paper [9] has suggested that, in youth at least, an optimally designed arterial structure includes the minimization of pulse wave reflections. The minimization of pulse wave reflections simultaneously minimizes central pulse pressure and maximizes peripheral pulse wave flow and, hence, influences perfusion of target organs.

The seminal application of the physics of fluid dynamics, by Womersley [10, 11] to the relationships between pulsatile trunk and branch arterial flows, occurred in the mid-to-late 1950's. Womersley's physics relationships have been included in most major textbooks related to the dynamics of blood flow [12–17]. The Womersley analysis determined relationships between pulse wave reflection, pulse wave velocity and arterial luminal areas. His analysis, as reflected in his plots of reflection coefficient as a function of area ratio, was limited to arteries whose diameters were greater than about 6.7 mm (Womersley number greater than five). His results were based on the asymptotic expansion of Bessel functions (solutions to the Bessel equation which describes fluid flow wave propagation in a cylinder), which he included in tabulated form. Although the Womersley pulse wave analysis described the flow field's distribution across the diameter of the vessel, it did not explicitly include arterial stiffness.

A fundamental characteristic of the Womersley physics-based analysis, however, is the existence of a specific combination of arterial dimensions and pulse wave velocities which optimizes antegrade pulsatile flow into

the peripheral arteries. To be generally applicable to the pressure and flow linkages between macrocirculation and microcirculation, however, the physics relationships must explicitly include the stiffnesses of all arteries, large and small.

The physical entity which links macrocirculation and microcirculation is the arterial junction, which is most often a bifurcation. The pressure and flow patterns of waves impinging on bifurcations are fundamental to the relationships between pressure and flow in the macrocirculation and in the microcirculation [18–22]. There have been estimated to be [15, 23, 24] twenty to thirty generations, or stages, of cascaded bifurcations in progressing from the central arteries to the capillaries, representing billions of bifurcations. Hence, the optimal design of bifurcations is of fundamental importance to the homeostasis maintenance of pressure and flow throughout the vasculature.

At a vascular bifurcation, in general, part of an impinging pulse wave is transmitted across the junction in antegrade flow, while a part of the wave is reflected back in retrograde flow. The fraction of the wave which is reflected, as compared to that which impinges on the bifurcation, is termed the reflection coefficient. The reflection coefficient is defined by Eq. (1):

$$\text{Reflection Coefficient} = \frac{\text{Reflected Pulse Pressure}}{\text{Forward Pulse Pressure}} \quad (1)$$

A bifurcation's reflection coefficient is determined by the mismatch in the flow impedances on either side of the bifurcation [18–22]. If the impedance characterizing the trunk artery (into the bifurcation) is equal to the total impedance of the branch arteries (out of the bifurcation), then the reflection coefficient is zero. In this matched condition, the pulse pressure amplification associated with the bifurcation is zero and the total pulse flow out of the bifurcation is equal to that into the bifurcation. This condition of matched arterial impedances across bifurcations is, therefore, an optimum condition for pulsatile blood flow, and related nutrient provision, into target organs.

The physics relationship which quantifies a bifurcation's reflection coefficient, as a function of the arterial stiffnesses and luminal cross-sectional areas, may be derived from the mismatch in the arterial impedances on either side of the bifurcation. To focus the body of this analysis on the medical implications of the physics, the derivation of the generalized equation for a bifurcation's reflection coefficient is consigned to Appendix A.

The quantitative analysis of the role of bifurcations' reflections in the linkages between macrocirculation and microcirculation, calls for the definition of these terms. For

the purpose of this analysis the macrocirculation is defined as that portion of the arterial tree for which the arterial diameters are greater than 6 mm (see Appendix B for the supporting rationale). The microcirculation is defined as that for which arterial diameters are less than 1 mm. The region of the arterial tree for which the arterial diameter is less than 6 mm but greater than 1 mm is described as the “mesocirculation”.

2 Study Purpose

One purpose of this study was to develop physics-based relationships between hemodynamic flow in the larger central arteries and the smaller peripheral arteries, explicitly including the stiffnesses and dimensions of all arteries, large and small, and also including pulse wave reflections which occur at bifurcations. A second purpose was to quantify the optimum arterial bifurcation design which minimizes pulsatile wave reflection and, hence, minimizes central pulse pressure and maximizes peripheral pulse flow.

3 Methodology

The methodology applied in this analysis is based on the physics of wave propagation and impedance matching in compliant tubes. The physics of wave propagation includes both the pressure and flow waveforms through the ratio of pulse pressure to pulse flow which is the impedance to flow offered by a compliant tube. The analysis focuses on the relationships between the impedances on either side of arterial bifurcations, in the derivation of the pulse wave reflection inherent to arterial impedance mismatches. Such impedance mismatches are fundamental to the relationships between arterial morphology, pulse wave reflection and peripheral pulse flow. In order to focus the body of manuscript on the physical and medical implication of the analysis, the derivation of the physics equations is consigned to the Appendices.

3.1 Fundamental Physical Relationships Between Pulsatile Flow and Bifurcation Reflection

At arterial bifurcations in general, the portion of the pressure wave that is reflected is added to that impinging on the bifurcation, so the total pulse pressure in the bifurcation’s trunk artery is given by [19, 20] Eq. (2):

$$\begin{aligned} & \text{Pulse Pressure (Trunk)} \\ &= [1 + \text{Reflection Coefficient}] \\ & \quad * [\text{Forward Pulse Pressure (Trunk)}] \end{aligned} \quad (2)$$

Since pressure at any point in a fluid is equal in all directions, the total pulse pressure (the sum of forward

and reflected pulse pressures) in the trunk artery is also transmitted into each of its branch arteries. Hence, the pulse pressure into each of the branch arteries is given by [19, 20] Eq. (3):

$$\begin{aligned} & \text{Pulse Pressure (Branch)} \\ &= [1 + \text{Reflection Coefficient}] \\ & \quad * [\text{Forward Pulse Pressure (Trunk)}] \end{aligned} \quad (3)$$

The above simple Eqs. (1)–(3) show dependencies of arterial trunk and branch pulse pressures on wave reflection coefficients and apply to all regions of the vasculature. An increase in wave reflection at a bifurcation produces an increase in both trunk and branch pulse pressures.

Although there is substantial evidence that increased central (aortic) pulse pressure is a predictor of target organ damage, reduced peripheral blood flow, or ischemia, has also been identified [8, 25–27] as a contributor to such damage. At bifurcations, in general, the pulsatile flow that is reflected back on the forward pulse flow in the trunk artery is in the opposite direction to the forward flow. Hence, the net pulsatile flow in the trunk artery is the forward flow wave reduced by the reflected flow wave. The predicted net pulse flow in the trunk artery is given by [19, 20] Eq. (4):

$$\begin{aligned} & \text{Pulse Flow (Trunk)} \\ &= [1 - \text{Reflection Coefficient}] \\ & \quad * [\text{Forward Pulse Flow (Trunk)}] \end{aligned} \quad (4)$$

The total antegrade pulse flow into the branches or periphery of a bifurcation is predicted to be reduced by the amount of pulse flow that is reflected by the bifurcation. For symmetrical bifurcations, with the two branch arteries of equal luminal cross-sectional areas, the predicted pulse flow in each branch is given by [19, 20] Eq. (5):

$$\begin{aligned} & \text{Pulse Flow (Branch)} \\ &= [1 - \text{Reflection Coefficient}] \\ & \quad * [\text{Forward Pulse Flow (Trunk)}]/2 \end{aligned} \quad (5)$$

Equations (4) and (5) show the dependence of central and peripheral pulse wave flows on bifurcations’ reflection coefficients. An increase in reflection coefficient produces a decrease in both central and peripheral pulse flow.

The fundamental principle which the above relationships identify is that, while increased bifurcation reflections increase central pulse pressure, they simultaneously decrease peripheral pulse flow. Although the above relationships are well established in the physics and engineering domains, they appear to be relatively unknown in the medical community, and hence are presented here as relatively new fundamental medical principles.

4 Results

Quantitative results obtained by calculating and plotting Appendix Eqs. (44)–(48) in the macrocirculation, microcirculation and mesocirculation regions are provided below.

4.1 Quantification of Pulse Wave Reflections at the Macrocirculation's Iliac/Aorta Bifurcation

A plot of the reflection coefficient (calculated using Eqs. 39 and 44–48 in Appendix A), for the larger arteries of the macrocirculation (i.e., diameters greater than 6 mm), is shown in Fig. 1 (as a function of the bifurcation's *Pulse Wave Velocity Ratio/Area Ratio*). The *Area Ratio*, using Womersley's [11] convention, is the quotient of the total luminal cross-sectional area of the branch arteries (out of the bifurcation) divided by the area of the trunk artery (into the bifurcation). Similarly, as a surrogate measure of relative arterial stiffnesses on each side of the bifurcation, the *Pulse Wave Velocity Ratio* is the quotient of the velocity of pulse waves in the branch arteries divided by the velocity of the pulse wave in the trunk artery. In vitro measured [21] values of reflection coefficient are superimposed on the predicted bifurcation reflection coefficient plot in Fig. 1. An assumption which underlies both of the physics-predicted and the measured iliac/aortic bifurcation reflection is that the branch arteries are well matched to subsequent branch arteries, and that reflections from such sub-branch arteries are negligible. The condition in which sub-branch reflections are not negligible is discussed in Appendix C in relation to mismatched arterial bifurcations in the mesocirculation. In Fig. 3, the absolute value of reflection coefficient

is used, consistent with standard physics (and Womersley's) conventions.

The generalized, physics-based reflection coefficient equations (Appendix Eqs. 44–48) extend Womersley's [11] reflection coefficient analysis, to specifically include the small arteries of the microcirculation, and to also explicitly include arterial stiffnesses. The bifurcation reflection coefficient plot of Fig. 1, applicable to the macrocirculation case (arteries greater than about 6 mm diameter), is consistent with Womersley's [11] bifurcation reflection plots (Womersley's plots displayed reflection coefficient as a function of area ratio for three different assumed values of relative pulse wave velocities).

In Fig. 1, the (absolute) values of in vitro measured [21] reflection coefficient data (as measured on aorta/iliac bifurcation cadaveric sections and as superimposed on the predicted reflection coefficient plot) were based on Womersley's analysis approach. In comparison, the reflection coefficient plot of Fig. 1 is that predicted using the generalized equations described in the Appendix (Eqs. 39 and 44–48). The match between the physics-based reflection coefficient plot and the measurement data indicates consistency between the bifurcation reflection coefficient equations and the measured values of pulse wave reflection coefficient for the macrocirculation's aorta/iliac bifurcation.

The reflection coefficient plot of Fig. 1 shows a very distinct reflection minimum which represents the optimum impedance match (with minimal central pulse pressure and maximal peripheral pulse flow). The optimum match occurs under the specific condition that:

$$\begin{aligned} & \text{Pulse Wave Velocity Ratio (Branch/Trunk)} \\ & = \text{Area Ratio (Branch/Trunk)} \end{aligned} \quad (6)$$

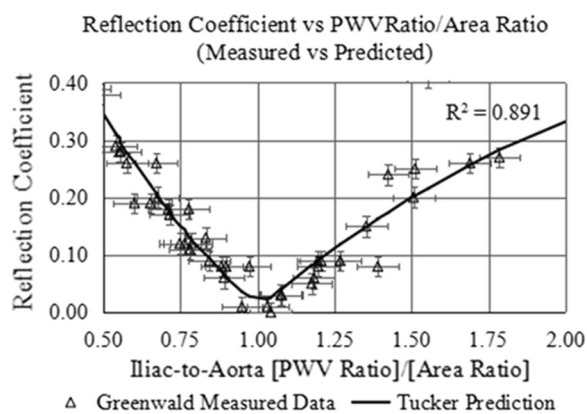


Fig. 1 Pulse wave reflection coefficient, in the macrocirculation, as a function of the quotient of the iliac-to-aorta pulse wave velocity ratio (PWVR) divided by the areas ratio (experimentally measured data from Greenwald et al. [21] and solid line is that predicted by this analysis)

The plot of Fig. 1 indicates that a variation in the *Pulse Wave Velocity Ratio/Area Ratio* of 25%, relative to that for minimal reflection, results in an increase in a pulsatile wave's reflection coefficient from near zero to about 12%. From Eq. (2) this increase in pulsatile reflection (without a change in the forward wave pressure) would therefore increase the central pulse pressure also by about 12%, and would simultaneously decrease peripheral pulse flow by about 12%. At the minimum point in the wave reflection coefficient plot, the central (aortic) pulse pressure is minimized and represents the optimum bifurcation design.

4.2 Arterial Stiffness Ratio in Relation to Pulse Wave Velocity Ratio

To eliminate the dependence of the measure of stiffness on the arterial luminal area (and, hence, include the resistive influence of viscosity) the arterial stiffness is here defined by Eq. (7) (see Appendix Eq. 24):

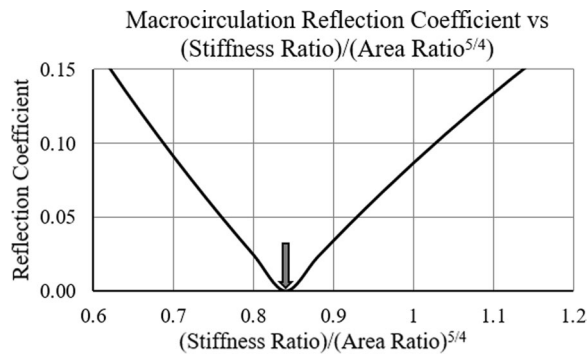


Fig. 2 Predicted macrocirculation bifurcation reflection coefficient as a function of the quotient of *Stiffness Ratio (Branch/Trunk)* divided by *Area Ratio (Branch/Trunk)^{5/4}*. Arrow indicates optimum bifurcation design (minimum reflection)

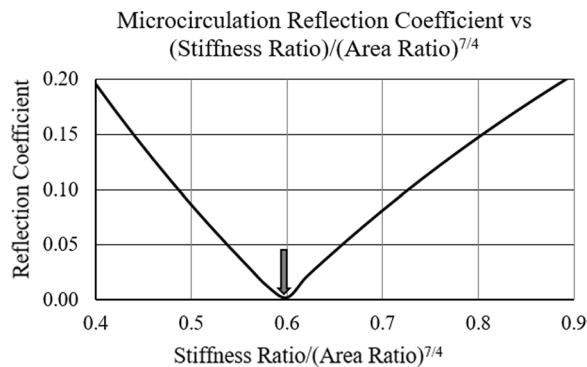


Fig. 3 The plot of the predicted microcirculation bifurcation reflection coefficient as a function of the quotient of branch-to-trunk $(Stiffness\ Ratio)/(Area\ Ratio)^{7/4}$

$$\begin{aligned}
 [Arterial\ Stiffness]^2 &= [Arterial\ Wall\ Thickness \\
 &\quad *Elastic\ Modulus * Blood\ Density * 2]/3
 \end{aligned}
 \quad (7)$$

Defining the arterial stiffness using only the material parameters of the arterial wall's thickness and elastic modulus, and the blood's density, provides a general definition of the stiffness of a bifurcation's arteries, which is independent of arterial diameters. This definition of arterial stiffness inherently includes the effect of viscosity and is valid for arbitrarily small values of luminal area (with the possible exception of arteries sufficiently fine that the Fahraeus–Lindqvist effect is significant).

In the large arteries of the macrocirculation, the relationship between the *Stiffness Ratio (Branch/Trunk)* and the *PWV Ratio (Branch/Trunk)*, is as shown in Eq. (8) (see the Appendix A for the derivation),

$$\begin{aligned}
 Stiffness\ Ratio\ (Branch/Trunk) &= PWV\ Ratio\ (Branch/Trunk) \\
 &\quad * [Area\ Ratio\ (Branch/Trunk)]^{\frac{1}{4}}
 \end{aligned}
 \quad (8)$$

In medical practice the arterial pulse wave velocity (which assumes negligible blood viscosity) is most often used as an indicator of an artery's stiffness even though PWV is dependent on arterial dimensions and is often applied for small arteries, for which viscous friction is not negligible.

4.3 Quantification of Wave Reflection at a Generalized Macrocirculation Bifurcation

The predicted reflection coefficient for bifurcations in the macrocirculation (i.e., for arterial trunk diameters greater than about 6 mm), is shown in the plot of Fig. 2 (calculated using Appendix A Eq. 33). The reflection coefficient of Fig. 2 is a function of the bifurcation's *Stiffness Ratio/Area Ratio^{5/4}* (as opposed to *PWV Ratio/Area Ratio*). The optimum design, which corresponds to the minimum in reflection, is indicated by an arrow in Fig. 2. The minimum reflection coefficient for bifurcations in the macrocirculation, representing optimum design, is predicted to be less than 0.1%.

The optimum impedance match, or minimum in the reflection coefficient plot, as indicated in Fig. 2 for macrocirculation bifurcations, occurs for the condition expressed by Eq. (9):

$$\begin{aligned}
 Stiffness\ Ratio\ (Macro\ Branch/Trunk) &= [2]^{-1/4} * [Area\ Ratio\ (Macro\ Branch/Trunk)]^{5/4}
 \end{aligned}
 \quad (9)$$

Equation (9) predicts that, if the aortic trunk stiffens relative to its branch arteries, then to maintain optimum homeostasis in pulse pressure and flow, the autonomic processes must increase the luminal area of the trunk relative to that of the branches. In the macrocirculation, if a central artery stiffens by 25%, (without significant reduction in autonomic regulation due to atheroma development or other vascular or neurovascular disease) then the central artery's luminal area should dilate by about 20% in order to maintain homeostasis in pulse pressure and flow. Atheroma development, or other arterial disease, which alters the optimum bifurcation design may significantly increase both central and peripheral pulse pressure and decrease peripheral pulse flow.

4.4 Quantification of Pulsatile Wave Reflection at a Microcirculation Arterial Bifurcation

The reflection coefficient for bifurcations in the microcirculation (for which the diameter of the bifurcation's trunk artery is less than about 1 mm), calculated using

Appendix A Eq. (38), is shown in the plot of Fig. 3 (as a function of the bifurcation's *Stiffness Ratio/Area Ratio*^{7/4}). The optimum design or minimum reflection coefficient value, for a single microcirculation bifurcation, is predicted to be less than 0.1%.

The minimum, or optimally matched condition in the microcirculation's reflection coefficient, as shown in Fig. 3, occurs for the condition identified by Eq. (10):

$$\begin{aligned} & \text{Stiffness Ratio (Micro Branch/Trunk)} \\ &= [2]^{-3/4} * [\text{Area Ratio (Micro Branch/Trunk)}]^{7/4} \end{aligned} \quad (10)$$

The plots of Figs. 2 and 3 are new and unique to this analysis yet are as fundamental as “Murray's Scaling Law” which is discussed in more detail in subsequent sections of the manuscript.

An optimally matched bifurcation in the microcirculation means that, with an area ratio that is greater than unity, the stiffness ratio may be less than unity. This property of the microcirculation's bifurcations means that, in proceeding through multiple generations of cascaded bifurcations, from the more central arteries into the arterioles and capillaries, with the attendant increase in total arterial area, successive generations may also increase in compliance (decrease in arterial stiffness).

Although the optimum reflection from a single microcirculation bifurcation may be small (less than 0.1%), there are many generations of cascaded bifurcations between the 1 mm diameter (largest microcirculation) artery to the smallest 7-micron diameter capillary. Combined reflected waves from many generations of cascaded bifurcations may present a potentially significant aggregate reflection coefficient, particularly in the presence of small vessel disease. In youth (i.e., 20–30 years) and good health, however, (and with optimum design) the microcirculation's contribution to central wave reflection and pulse pressure is predicted to be relatively small. With small vessel disease, a relatively small increase in the reflection coefficients of a number of cascaded bifurcations, may result in significant combined wave reflection, with accompanying central pulse pressure increase and peripheral pulse flow decrease.

4.5 Quantification of Pulsatile Wave Reflection at a Mesocirculation Bifurcation

Near the centre of the mesocirculation region, with an assumed mean stiffness ratio of near unity, the reflection coefficient for a bifurcation is predicted to be a function of area ratio and stiffness ratio, as shown in Fig. 4 (for a bifurcation with trunk diameter=3 mm). In the mesocirculation, the region in which the stiffness ratio

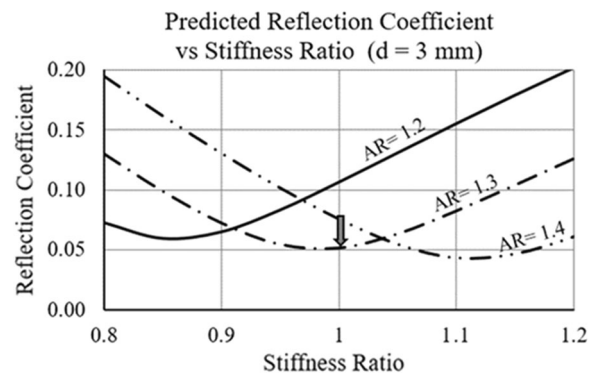


Fig. 4 Predicted reflection coefficient, near the center of the mesocirculation region (for a 3 mm diameter trunk artery), as a function of the Stiffness Ratio, for three different values of Area Ratio. The arrow at stiffness ratio $SR=1.0$

transitions from a value of greater than unity (for bifurcations proximal to the macrocirculation region), to a value that is less than unity, (for bifurcations proximal to the microcirculation) an average stiffness ratio of approximately one is indicated. As shown in Fig. 4, the optimum reflection coefficient, near the middle of the mesocirculation region, has a finite value of approximately 0.05 or 5%. In the mesocirculation, wave reflection is predicted even in the case of optimum bifurcation design. The physical cause of this finite reflection coefficient in the mesocirculation is that the in-phase, resistive contribution to the reflection coefficient and the orthogonal, or out-of-phase, inertial/compliant contribution are both finite and not simultaneously matched. For a mesocirculation bifurcation, this analysis predicts that the optimum arterial match does not reduce to the low levels of the optimum match for bifurcations in the macrocirculation and the microcirculation (which may optimally be less than 0.1%). The mesocirculation reflection coefficient, which is predicted to be in the 4–6% range, represents an optimum value, irrespective of autonomic vasodilation processes. Although there may be relatively few generations of mesocirculation bifurcations, each is indicated to make a significant contribution to the aggregate of reflections from all arterial regions, macrocirculation, mesocirculation and microcirculation.

The finite reflection coefficient for bifurcations in the mesocirculation, results in an essential impedance mismatch between the macrocirculation and microcirculation regions. This impedance mismatch between macro and microcirculation regions results in wave reflection in the central arteries, including the aorta. Because the central pulse pressure is the sum of the forward and reflected wave pressures the central (aortic) pulse pressure is

predicted to be substantially dependent on the amount of mesocirculation bifurcation reflection.

If arterial stiffnesses or luminal areas change from optimum values in youth, through aging, through atheroma development or through other vascular diseases, then the central pulse pressure is predicted to increase, potentially significantly, particularly if a number of generations of arterial bifurcations are sclerotic or diseased.

4.6 Estimation of Optimum Aggregate Mesocirculation Reflection

The minimum reflection coefficient plots for bifurcations in the macrocirculation, as shown in Figs. 1 and 2, are based on the load impedances at the distal end of each of the bifurcation’s branches being matched to the characteristic impedance of each branch (i.e., if the branch is well matched to its sub-branches). If, however, the branch is mis-matched at its distal end, then that mismatch is transformed along the branch to its proximal end at the bifurcation (see Appendix C). To a first order of approximation, this sub-branch reflection transforms the reflection coefficient at a primary trunk-to-branch bifurcation to that of the mismatch at the distal end of the branch arteries.

Figures 4 and 13 (Appendix B) indicate that near the centre of the mesocirculation region, which corresponds to an arterial diameter of about 2–4 mm, the optimum reflection coefficient for that centre bifurcation is in the range of 4–6%. With eight symmetric bifurcations in the mesocirculation, to attain 4% in the centre of the mesocirculation, implies, each successive bifurcation increments the reflection by 1%. With each branch in the mesocirculation sequentially mismatched by about 1%, the total mismatch, or aggregate reflection coefficient for eight bifurcations, is estimated to be about 21.7% ($1.01 \cdot 1.02 \cdot 1.03 \cdot 1.04 \cdot 1.04 \cdot 1.03 \cdot 1.02 \cdot 1.01 = 1.217$). To attain 6% reflection in the centre of the mesocirculation region,

each successive bifurcation increments by 1.5% which yields, by a similar calculation, an aggregate reflection coefficient for the mesocirculation of about 31.4%. The prediction that the mesocirculation generates the greatest pulse wave reflection in the central arteries is a fundamental new assessment of an otherwise elusive effective reflection site. A maximum reflection coefficient of 34% from arteries with diameters in the 3–4 mm range was also predicted by Pollock [28].

Even in youth and good health, with assumed optimum arterial impedance matching, there is predicted to be finite wave reflection in the macrocirculation caused by essential mismatches in mesocirculation bifurcations. A minimum central artery reflection coefficient in the range of 22–31% is predicted from inherent mesocirculation mismatch. In optimal mesocirculation bifurcation design, this inherent mismatch represents a minimum in central (aortic) pulse pressure and a maximum in peripheral (microcirculation) pulse flow.

4.7 Optimum Combinations of Arterial Dimensions and Stiffnesses

Figure 5 provides plots of the optimum combinations of bifurcations’ stiffnesses and area ratios corresponding to minimal pulse wave reflection in the two limiting cases of the macrocirculation (see Eq. 9) and the microcirculation (see Eq. 10). The circled area in Fig. 5, corresponds to the optimum conditions in which the stiffness ratio transitions from greater than unity in the macrocirculation, to less than unity in the microcirculation, with the case of $SR = 1.0$ centered between the two limiting cases.

In youth and good health, the aorta is more compliant than the aortic branch arteries. However, also in youth and good health, in the smaller arteries, (i.e., the microcirculation) the branch arteries must be more compliant than their trunk arteries to ensure the arterioles are substantially more compliant than the more central arteries.

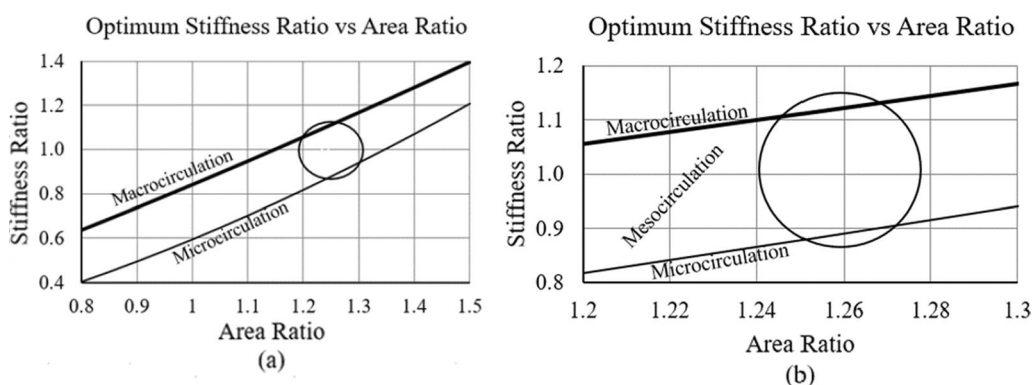


Fig. 5 a Optimum Stiffness Ratio as a function of Area Ratio for a minimum in bifurcation reflection coefficient for the two limiting cases of macrocirculation and microcirculation; b expanded plot of Fig. 10a with an optimum match in the centre of the mesocirculation region indicated

The circled area is centered on a stiffness ratio of unity ($SR=1.0$) which corresponds to the arterial stiffness ratio near the centre of the mesocirculation region.

Figure 5 shows that the area ratios in both the macrocirculation and in the microcirculation have a value of approximately $AR=1.26$ for the condition that the stiffness ratio of $SR=1.0$ lies at the centre of the mesocirculation region. Figure 5 demonstrates that the stiffness ratio (SR) in the macrocirculation region which corresponds to an area ratio of $AR=1.26$, is approximately $SR=1.12$. In the macrocirculation, for which arterial diameters are greater than about 6 mm, the arteries become stiffer (in youth at least) in progressing from the aorta into the aortic branch arteries. In the microcirculation, the stiffness ratio corresponding to $AR=1.26$ is about $SR=0.89$. In the microcirculation, in proceeding from generation to generation of cascaded microcirculation bifurcations, the total area of the arterial bed increases while the arterial stiffness decreases.

The optimum area ratio in the mesocirculation is predicted to vary from the value of $AR=1.26$ which is applicable to the macro and microcirculation regions. In the mesocirculation, the stiffness ratio varies from $SR=1.12$ proximal to macrocirculation to $SR=0.89$ proximal to the microcirculation. At the stiffness ratio of unity ($SR=1.0$) the Area Ratio which corresponds to an optimum match is in the range of about $AR=1.26$ – 1.31 (see Fig. 4).

An area ratio of $AR=1.26$ corresponds to the diameter of each bifurcation's branch being approximately 79% of that of its trunk artery. In the microcirculation, at each level, or generation, in a progression of cascaded bifurcations, while the diameter of individual branch arteries reduces, the stiffness of those arteries simultaneously reduces. Hence, in the microcirculation, the analysis predicts that, while the total cross-sectional area of the arterioles and capillaries may be substantially greater than that of the central arteries, they may also, simultaneously, be substantially more compliant. This prediction is consistent with the human vascular physiology.

4.8 Quantification of the Number of Generations of Cascaded Bifurcations

The number of generations of bifurcations which occur in the microcirculation and the mesocirculation regions is much greater than in the macrocirculation. In the macrocirculation, between the brachiocephalic trunk artery (diameter typically 14 mm) and the internal carotid artery (diameter typically 6–7 mm), there are typically two generations of (asymmetric) bifurcations. For an optimum macrocirculation bifurcation area ratio of 1.26, the optimum stiffness ratio is about 1.12. In two macrocirculation bifurcations the stiffness of a 6 mm diameter distal artery would be about 1.25 (1.12^2) times that of the aorta.

Two generations of bifurcations are a small fraction of the estimated [15, 23, 24] twenty to thirty generations of cascaded bifurcations which occur in a single vascular tree extending from the central arteries to the capillaries.

For mesocirculation bifurcations, each with an assumed area ratio of about 1.3 (for which the diameter of a branch artery is about 81% of the trunk artery), eight generations of bifurcations are required to reduce a 6 mm trunk into a 1 mm branch. In the mesocirculation the stiffness ratio transitions from a value of about 1.12, proximal to the macrocirculation, to a value of about 0.89, proximal to the microcirculation.

For microcirculation bifurcations, each with an assumed area ratio of about 1.26, twenty generations of bifurcations are required to reduce a 1 mm diameter trunk to a 9 micron diameter capillary. With a stiffness ratio of about 0.89 for each microcirculation bifurcation, the stiffness of the capillaries is predicted to be a factor of about one tenth (0.89^{20}) that of the microcirculation arteries which are proximal to the mesocirculation.

Hence, with two generations of bifurcation in the macrocirculation, eight generations in the mesocirculation and twenty generations in the microcirculation, there are estimated to be about thirty generations, (based on the simplifying assumption of junction symmetry) of bifurcations between the aorta and the capillaries.

The optimum value of bifurcation reflection coefficient in the macrocirculation is less than 0.1%. Hence, in two generations of optimally designed macrocirculation bifurcations, wave reflection is negligible, and the pulse wave flow out of the macrocirculation is approximately equal to that in the aorta. The value of bifurcation reflection coefficient in the mesocirculation varies between a low of close to zero to a maximum in the range of about 4–6%. The aggregate reflection coefficient for the mesocirculation, assuming coherent summing of the reflections, is predicted to be in the range of about 22–31%. The percentage of total antegrade pulse flow from the mesocirculation into the microcirculation is, therefore, predicted to be in the range of about 69–78% of that in the aorta.

The value of reflection coefficient for a single, optimally designed, bifurcation in the microcirculation is less than 0.1%. Hence, in about twenty-two generations of optimally designed bifurcations in the microcirculation, less than 3% ($1-0.999^{22}$) of the pulse wave emerging from the mesocirculation is reflected and more than 97% flows into the capillaries. Hence, the optimum or maximum total antegrade pulse wave flow into the capillaries is in the range of about 66–75% of that from the aorta. The largest single contributors to wave reflections in a well-matched arterial tree are predicted to be those arteries in

the mesocirculation whose diameters are in the range of 2–3 mm, and whose stiffness ratios are near unity.

Any bifurcation in the arterial tree in which impedance match is not maintained by autonomic processes, perhaps as a result of atheroma development or a result of other vascular or neurovascular diseases, will impact wave flow downstream of such bifurcation mismatch, flow into the distal capillaries in that entire arterial branch.

Figure 6 shows the predicted arterial diameter, arterial stiffness, and total arterial bed area, relative to the aorta, for thirty generations of arterial bifurcations. The total arterial bed area is predicted to increase about one thousand times (i.e., the total capillary bed area is about one thousand times greater than that of the aorta), while the individual arterial size is predicted to decrease by about one thousand times, each relative to the aorta. The stiffness ratio is predicted to increase slightly in the macrocirculation and until about the mid-point of the mesocirculation, at which point it begins to decrease. The stiffness of the first branch of the microcirculation, as shown, in Fig. 6, is predicted to be about the same value as the stiffness of the aorta. The stiffness of the arteries in the microcirculation decrement by about 11% for each generation of bifurcation progressing into the capillaries. The stiffness of the capillaries is predicted to be about one tenth (0.89²⁰) that of the aorta.

4.9 Bifurcation Cascades and “Murray’s Scaling Law”

An alternate means of estimating the number of cascaded bifurcations between the aorta and the capillaries arrives at a similar set of estimates (i.e., about 30 generations of bifurcations, with an average Area Ratio ≈ 1.26). The total arterial area of the capillaries is historically reported [15, 23, 24] to be about one thousand times that of the central arteries, while the central arteries are historically reported [15, 29, 30] to be about thirty times stiffer than

the veins. If autonomic adaptation processes modulate stiffness ratios and arterial area ratios to maintain flow homeostasis, then in “n” generations of cascaded bifurcations the total area of the capillary bed may be represented by Eq. (11):

$$\begin{aligned} \text{Total Area Ratio (Capillary Bed/Central)} \\ = [\text{Average Area Ratio (Branch/Trunk)}]^n \approx 1000 \end{aligned} \tag{11}$$

In addition, assuming the arterial stiffness decrease from the capillaries to the central veins is comparable to that from the central arteries to the capillaries, the stiffness relationship between the central arteries and the capillaries may be expressed by Eq. (12):

$$\begin{aligned} \text{Stiffness Ratio (Capillaries/Central)} \\ = [\text{Average Stiffness Ratio (Branch/Trunk)}]^n \approx 1/15 \end{aligned} \tag{12}$$

The above three Eqs. (10), (11) and (12) can be solved for the three unknowns, “n”, “Average Stiffness Ratio (Branch/Trunk)” and “Average Area Ratio (Branch/Trunk)”. An Average Area Ratio=1.26, which is bifurcated 30 times produces a total arterial bed result of about 1000 (1.26³⁰=1026). This method of estimating average area ratio, as discussed by Zamir [15], produces an almost identical result to that based on the minimal pulse wave reflection principle discussed above.

The classic “Murray’s Law” [31] of arterial bifurcation area ratios, which has been widely addressed in many of the standard texts on blood flow [12, 15–17], offers a “scaling law” for the dimensions of arteries at symmetric bifurcations for which the area ratio is given by Area Ratio=2^{1/3}=1.26. This analysis, which is based on the principle of minimizing the magnitude of pulsatile waves reflected from bifurcations, produces a scaling law apparently identical to Murray’s Law, which is based on the principle of minimizing the work required to move nonpulsatile blood flow through bifurcations. Although Murray’s Law does not include the influence of arterial stiffnesses on the optimum bifurcation impedance match, this analysis indicates there is an influence of such arterial stiffness in minimizing wave reflection. This analysis indicates that an idealized impedance match can be maintained in bifurcations for which the Area Ratio is other than 1.26, if autonomic vasodilation processes adjust the arterial stiffnesses in compensation. Such arterial stiffness compensation processes are not predicted by the Murray analysis approach.

Fundamental new “Scaling Laws” which incorporate the arterial stiffness ratios are developed in this analysis, one applicable to the macrocirculation and another applicable to the microcirculation. For the macrocirculation, Eq. (9) can be rewritten as the scaling law of Eq. (13):

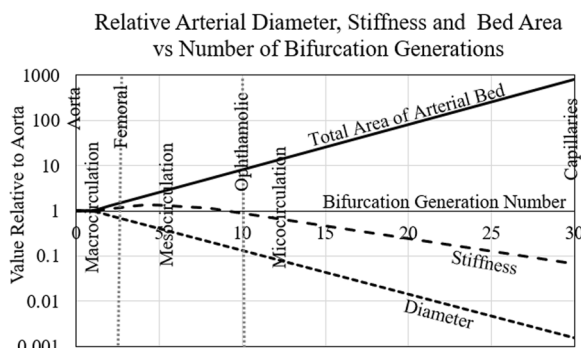


Fig. 6 The relative (to the aorta) arterial diameter, arterial stiffness, and total area of the arterial bed at each generation of bifurcation in progressing from the aorta to the capillaries

$$Area\ Ratio = 2^{1/5} * [Stiffness\ Ratio]^{4/5} \tag{13}$$

Under the specific macrocirculation condition that $Stiffness\ Ratio = 2^{1/6} = 1.12$, the $AreaRatio = 2^{1/3}$, which matches Murray’s Law.

For the microcirculation, Eq. (10) can be rewritten as the scaling law of Eq. (14):

$$Area\ Ratio = 2^{3/7} * [Stiffness\ Ratio]^{4/7} \tag{14}$$

Under the specific microcirculation condition that $Stiffness\ Ratio = 2^{-1/6} = 0.89$, the $AreaRatio = 2^{1/3}$, also matching Murray’s Law.

Two additional, slightly different, arterial area scaling laws, the Huo–Kassab Law [32] and the Finet Law [33] have also been identified. The scaling laws developed in this analysis are more general than the Murray, Finet or Huo–Kassab Laws, in that the laws developed here explicitly include the influence of arterial stiffness. Each of the previous three scaling laws represents a specific case of the new scaling laws for specific equivalent values of stiffness ratio. Table 1 below identifies each of the three previous scaling laws (for the symmetric bifurcation case) and the specific values of stiffness ratio in both the macrocirculation and the microcirculation which provide equivalence to the new scaling laws developed here.

4.10 Comparison of Predicted and Measured Wave Reflection Coefficient

Table 2 summarizes reflection factor measurement data taken using various measurement techniques. The term reflection factor is applied in Table 2 as a generalization of the term reflection coefficient. This generalization is intended to reflect the different measurement techniques and calculations applied, and for consistency with a number of the references in the table.

The average value of measured aggregate reflection factor in Table 2, is 30.9%, with a standard deviation of 10.8%. Given that the measured data includes that taken in various arteries and in elderly patients with attendant atheroma and other vascular diseases, the average value of measured reflection factor is expected to be greater

than that for youthful patients in good health and is also expected to be heterogeneous.

The minimum, or idealized, aggregate reflection coefficient from multiple bifurcations in the mesocirculation, as discussed in the Sect. “4.6” is predicted to be in the range of 21.7–31.4%. Measured values for reflection factor that are greater than this idealized range may be interpreted as representing impedance mismatches associated with arteriosclerotic, stenotic or aneurysm development or other vascular diseases. Values that are less than this idealized range may be interpreted as either measurements on a single bifurcation (as opposed to the aggregate of a cascade of bifurcations) or a consequence of such influences as the turbulent mixing of forward and reverse flow waves, and other measurement-related inaccuracies. As discussed in the Sect. “4.1” a variance in $PWV\ Ratio/Area\ Ratio$ from the ideal value results in a direct increase in reflection coefficient in a single bifurcation. Similarly, variance from the ideal impedance match in cascaded bifurcations will accumulate in significant increases to the aggregate reflection coefficient.

The ratio of measured peak reverse-to-forward flows, as indicated in Table 2, tended to have lower reflection factor values than similar ratios of pressure or velocity measurements, potentially as a result of simultaneous forward and reverse flows with turbulent mixing across a luminal area. Such flow mixing will affect the interpretation of forward and reverse flows, resulting in a reduction in apparent net flow, leading to an underestimation of reflection coefficient. The pulse wave separation (forward and reverse pressure waves) analysis technique used for pressure ratio computations resulted in substantial heterogeneity in the calculated reflection coefficient, perhaps as a consequence of the different measurement techniques used and the difficulty of accurately separating the contributions of the forward and reversed pressure waves to the combined pressure wave.

The calculated reflection factor associated with the ratio of measured peak reverse to forward velocities resulted in a more uniform set of measured results than either the flow or pressure ratio measurements. The reflection factors measured using the peak velocities ratio, of middle-aged patients (45–55 years), as indicated

Table 1 Values of Stiffness Ratios which provide equivalence of the scaling laws developed here to the previously developed Murray [31], Huo–Kassab [32] and Finet [33] scaling laws

Scaling Law	Macrocirculation	Microcirculation	AR	Equivalent SR_{Macro}	Equivalent SR_{Micro}
This analysis	$AR = 2^{1/5} * [SR]^{4/5}$	$AR = 2^{3/7} * [SR]^{4/7}$	1.26	1.12	0.89
Murray [31]	$AR = 2^{1/3}$	$AR = 2^{1/3}$	1.26	1.12	0.89
Huo–Kassab [32]	$AR = 2^{1/7}$	$AR = 2^{1/7}$	1.10	0.95	0.74
Finet [33]	$AR = 1.09$	$AR = 1.09$	1.09	0.93	0.69

Table 2 Measured reflection factor data. In vivo measurement methods included the tonometric measurement of pressure and the Doppler ultrasound, phase contrast MRI and 4D flow MRI measurement of peak velocity and peak flow ratios

References	Patient age and gender	Artery	Type	Method	Equation	Reflection factor RF \pm SD (%)	Comment
Greenwald et al. (1990) [21]	<50 Mixed	Abdominal aorta	In vitro	Intra-lumen transducer	$\frac{1-2AR/PWVR}{1+2AR/PWVR}$	10 \pm 4	Iliac/aorta bifurcation only
Greenwald et al. (1990) [21]	>50 Mixed	Abdominal aorta	In vitro	Intra-lumen transducer	$\frac{1-2AR/PWVR}{1+2AR/PWVR}$	10 to 30 \pm 8	Iliac/aorta only RF increases with age
Yamamoto et al. (1996) [34]	48 \pm 20 Mixed	Renal	In vivo	Doppler ultrasound	$\frac{Velocity_{PeakReverse}}{Velocity_{PeakForward}}$	30 \pm 10	Vortical, mixed reverse and forward
Mitchell et al. (2003) [35]	58 \pm 9 Male	Carotid	In vivo	Tonometry	$\frac{Pressure_{PeakReverse}}{Pressure_{PeakForward}}$	13 \pm 5	RF increases with age
Mitchell et al. (2003) [35]	57 \pm 9 Female	Carotid	In vivo	Tonometry	$\frac{Pressure_{PeakReverse}}{Pressure_{PeakForward}}$	22 \pm 8	RF increases with age
Mitchell et al. (2010) [36]	37 \pm 7 Mixed	Proximal aorta	In vivo	Tonometry, Doppler US	$\frac{Pressure_{PeakReverse}}{Pressure_{PeakForward}}$	34 \pm 6	Healthy controls, RF increase with age
Hashimoto and Ito (2010) [37]	56 \pm 13 Mixed	Femoral	In vivo	Tonometry, Doppler US	$\frac{Velocity_{PeakReverse}}{Velocity_{PeakForward}}$	28 \pm 10	RF decreases with increased aortic PWV
Hashimoto et al. (2011) [38]	56 \pm 12 Mixed	Femoral	In vivo	Tonometry, Doppler US	$\frac{Velocity_{PeakReverse}}{Velocity_{PeakForward}}$	30 \pm 10	RF increase with increased Pourcelot index
Mitchell et al. (2011) [39]	76 \pm 4 Mixed	Carotid	In vivo	Tonometry	$\frac{Pressure_{PeakReverse}}{Pressure_{PeakForward}}$	6 \pm 3	Carotid/aorta bifurcation only
Hashimoto and Ito (2013) [40]	54 \pm 13 Mixed	Thoracic aorta	In vivo	Tonometry, Doppler US	$\frac{Velocity_{PeakReverse}}{Velocity_{PeakForward}}$	35 \pm 10	Reflection increases with PWV gradient
Coutinho (2013) [41]	67 \pm 9 Male	Carotid	In vivo	Tonometry, Doppler US	$\frac{Pressure_{PeakReverse}}{Pressure_{PeakForward}}$	36 \pm 13	cfPWV = 11.9 \pm 3.8
Coutinho et al. (2013) [41]	65 \pm 9 Female	Carotid	In vivo	Tonometry, Doppler US	$\frac{Pressure_{PeakReverse}}{Pressure_{PeakForward}}$	37 \pm 13	cfPWV = 10.5 \pm 3.4
Bensalah et al. (2014) [42]	27 \pm 6 Mixed	Ascending aorta	In vivo	PC MRI	$\frac{Flow_{PeakReverse}}{Flow_{PeakForward}}$	11 \pm 4	Vortical, mixed reverse and forward
Bensalah et al. (2014) [42]	54 \pm 9 Mixed	Ascending aorta	In vivo	PC MRI	$\frac{Flow_{PeakReverse}}{Flow_{PeakForward}}$	18 \pm 7	Vortical, mixed reverse and forward
Torjesen et al. (2014) [43]	51 \pm 15 Male	Central (Aorta?)	In vivo	Tonometry, Doppler US	$\frac{Pressure_{PeakReverse}}{Pressure_{PeakForward}}$	34 \pm 6	RF increases with age
Torjesen et al. (2014) [43]	51 \pm 16 Female	Central (Aorta?)	In vivo	Tonometry, Doppler US	$\frac{Pressure_{PeakReverse}}{Pressure_{PeakForward}}$	36 \pm 7	RF increases with age to 55, decreases after age 55
Hashimoto and Ito (2015) [44]	52 \pm 12 Mixed	Proximal aorta	In vivo	Doppler US eGFR > 60	$\frac{Velocity_{PeakReverse}}{Velocity_{PeakForward}}$	33 \pm 10	Increased RF decreases eGFR
Hashimoto and Ito (2015) [44]	58 \pm 13 Mixed	Proximal aorta	In vivo	Doppler US eGFR < 60	$\frac{Velocity_{PeakReverse}}{Velocity_{PeakForward}}$	38 \pm 10	Increased RF decreases eGFR
Breton et al. (2016) [45]	40 \pm 10 Mixed	Brachial	In vivo	Tonometry, Doppler US	$\frac{Velocity_{PeakReverse}}{Velocity_{PeakForward}}$	24	RF and PWVR increase with age
Breton et al. (2016) [45]	61 \pm 9 Mixed	Brachial	In vivo	Tonometry, Doppler US	$\frac{Velocity_{PeakReverse}}{Velocity_{PeakForward}}$	54	RF and PWVR increase with age
Kim et al. (2017) [46]	59 \pm 12 Mixed	Descending aorta	In vivo	Tonometry, Doppler US	$\frac{Velocity_{PeakReverse}}{Velocity_{PeakForward}}$	40 \pm 10	Pulse pressure (PP) PP < 71 mmHg
Kim et al. (2017) [46]	65 \pm 9 Mixed	Descending aorta	In vivo	Tonometry, Doppler US	$\frac{Velocity_{PeakReverse}}{Velocity_{PeakForward}}$	45 \pm 10	PP > 71 mmHg, RF and PP increase with age
Jue et al. (2019) [47]	62 + 12 Male	Carotid?	In vivo	Tonometry, Doppler US	$\frac{Pressure_{PeakReverse}}{Pressure_{PeakForward}}$	39 \pm 3	Aortic Aneurysm (AA) RF independent of AA
Jue et al. (2019) [47]	65 + 9 Female	Carotid?	In vivo	Tonometry, Doppler US	$\frac{Pressure_{PeakReverse}}{Pressure_{PeakForward}}$	46 \pm 10	RF increases with AA diameter increase

Table 2 (continued)

References	Patient age and gender	Artery	Type	Method	Equation	Reflection factor RF \pm SD (%)	Comment
London et al. (2019) [48]	54 \pm 2 Mixed	Carotid	In vivo	Tonometry	$\frac{Pressure_{PeakReverse}}{Pressure_{PeakForward}}$	26 \pm 2	Normotensive controls
London et al. (2019) [48]	54 \pm 1 Mixed	Carotid	In vivo	Tonometry	$\frac{Pressure_{PeakReverse}}{Pressure_{PeakForward}}$	41 \pm 1	Hypertensive, RF increases with PP
Evdochim et al. (2020) [49]	24, Single subject	Brachial	In vivo	Tonometry	$\frac{Pressure_{PeakReverse}}{Pressure_{PeakForward}}$	0 to 50	RF varies with mean pressure, RF = 0 at MAP = 100 mmHg
Jarvis et al. (2020) [50]	36 \pm 9 Mixed	Upper aorta	In vivo	4D Flow MRI	$\frac{Flow_{MeanReverse}}{Flow_{MeanForward}}$	8 \pm 3	Youthful controls, RF affected by mixed reverse, forward flow
Jarvis et al. (2020) [50]	65 \pm 8 Mixed	Upper aorta	In vivo	4D Flow MRI	$\frac{Flow_{MeanReverse}}{Flow_{MeanForward}}$	15 \pm 5	Age matched controls RF increase with PWV
Jarvis et al. (2020) [50]	69 \pm 9 Mixed	Upper aorta	In vivo	4D Flow MRI	$\frac{Flow_{MeanReverse}}{Flow_{MeanForward}}$	17 \pm 6	Stroke patients RF affected by mixed reverse, forward flow
Haidar et al. (2021) [51]	75 \pm 4 Mixed	Carotid and others	In vivo	Tonometry, Doppler US	$\frac{Flow_{PeakReverse}}{Flow_{PeakForward}}$	34 \pm 10	Asymmetric carotid-aorta bifurcation well matched
Haidar et al. (2021) [51]	75 \pm 4 Mixed	Carotid and others	In vivo	Tonometry, Doppler US	$\frac{Pressure_{PeakReverse}}{Pressure_{PeakForward}}$	41 \pm 11	Increased aorta stiffness decreases RF
Hashimoto et al. (2022) [52]	55 \pm 14 Mixed	Femoral	In vivo	Doppler US	$\frac{Velocity_{PeakReverse}}{Velocity_{PeakForward}}$	32 \pm 10	Ischemic organ damage with increased Reflection Factor

in Table 2, ranged from a low of about 30% \pm 10% in the renal artery to a high of about 45% \pm 10% in the descending aorta. These measured values of reflection factor (average value of 30.9% \pm 10%) compare reasonably favorably with the predicted optimum (or idealized) reflection coefficient range of 22–31% and with arterial variance in human physiology. In human physiology, reverse to forward wave ratio measurements are predicted to increase as a consequence of atheroma development or other vascular physiological irregularities. The measurement data of Table 2 indicates an increase in reflection factor with increasing age, irrespective of the measurement technique applied. Such an increase is consistent with increasing impedance mismatches which occur with aging, as arterial luminal areas reduce and vessel walls thicken with atheroma development, particularly at the ostia of macrocirculation and mesocirculation bifurcations.

5 Discussion

5.1 Medical Significance of Optimal Arterial Design and Structure

This analysis infers that in youth, and good health, bifurcations throughout the arterial tree are optimally

designed, structured, and tuned to minimize central pulse pressure and to maximize peripheral and capillary pulse flow. The simultaneous minimization of central pulse pressure and maximization of peripheral pulse flow is associated with optimizing arterial bifurcation design and structure throughout the vasculature.

The analysis also infers that arterial property changes, particularly changes in luminal areas or arterial wall stiffnesses, can significantly increase wave reflection at arterial bifurcations, causing increased central pulse pressure and decreased peripheral pulse flow. For cascaded bifurcations which are mismatched, the deleterious pressure and flow effects can be cumulative, and hence, substantial. There are many potential causes of such arterial property changes, including age-related arteriosclerosis, obesity, smoking, diabetes, vascular diseases, and neurovascular disorders. Autonomic regulatory processes, if unaffected by disease, would tend to mitigate the effects of such deleterious arterial changes through central pressure homeostasis maintenance, endothelial dependent vasodilation and neurovascular baroreflex regulation.

Clinical diagnoses and treatments traditionally focus on systolic, diastolic and pulse pressures, most often measured at the brachial artery. Pharmaceutical treatments

tend to emphasize the reduction of pulse pressure and mean arterial pressure through modulating the renin–angiotensin–aldosterone system (with such medications as angiotensin converting enzyme inhibitors, angiotensin receptor blockers and aldosterone receptor antagonists). Treatments also address atheroma development and arterial stiffness change through the use of pharmaceuticals such as statins, to reduce lipid deposition, and calcium channel blockers, but may also involve exercise regimes with dietary and smoking regulation.

Adverse cardiovascular events have been widely associated with stiffening of the central arteries, in particular, the aorta. The carotid-to-femoral pulse wave velocity (*cfPWV*) has been identified in several expert consensus reports [53–56] as the “gold standard” surrogate measure of central, or aortic, arterial stiffness (which is difficult to directly measure in vivo). Elevated *cfPWV*, or aortic “stiffening”, has been widely associated with hypertension, atheroma development, adverse cardiovascular events, and target organ damage.

Various reports [39, 56–59] have suggested that, with aging, the inversion of the central-to-peripheral arterial stiffness gradient increases the pulse pressure transmitted into target organs, causing organ damage. This analysis offers a prediction that is at some variance with the perception that the central artery’s stiffness exceeding that of the peripheral arteries causes increased pulse pressure in the peripheral arteries. This analysis indicates that a bifurcation impedance mismatch, involving both arterial stiffnesses and luminal areas, results in increased central pulse pressure (with a simultaneous decrease in peripheral pulse flow). The optimum combination of arterial stiffnesses and luminal areas is different in the three different regions of the vasculature. Although an arterial stiffness gradient that is associated with the central arteries being stiffer than the peripheral arteries may result in increased peripheral pulse pressure, the converse may also be true. Peripheral arteries which are much stiffer than central arteries can also result in increased pulse reflection and peripheral pulse pressure. The relative luminal areas of the central and peripheral arteries also affect the impedance mismatch at bifurcations and hence, peripheral pulse pressure.

5.2 A Prospective New “Gold Standard” for Arterial Stiffness Measurement

Some recent longitudinal studies [60–62] suggest that the ratio of central to peripheral pulse wave velocities may be a better predictor of adverse cardiovascular events than *cfPWV* alone and has also been suggested [63] as a possible “new gold standard” for the measurement of arterial stiffness. The ratio of central-to-peripheral pulse wave velocities is also often referred to as the arterial stiffness

gradient. This physics-based analysis predicts that the central-to-peripheral stiffness gradient is a better predictor of increased pulse pressure, and decreased pulse flow, than central arterial stiffness alone. This prediction has greater validity if the peripheral PWV measured is that of the femoral-to-ankle rather than that of the carotid-to-brachial arteries. When carotid-to-femoral PWV measurements are used to describe the aortic stiffness, then the femoral-to-ankle PWV offers a better indication of central-to-peripheral gradient arterial mismatch, than carotid-to-brachial or carotid-to-radial measurements, (since the relevant bifurcation in the pulse wave’s reflection is the iliac-to-femoral bifurcation). The Stone study [61] that used the femoral-to-ankle PWV for peripheral artery stiffness, reported a greater correlation with adverse cardiovascular events than the Fortier study [60] which used the carotid-to-brachial PWV measurement as the peripheral stiffness measurement.

This analysis predicts that the quotient of the ratio of peripheral to central pulse wave velocities divided by the ratio of peripheral to central luminal areas (i.e., *Pulse Wave Velocity Ratio/Area Ratio*) is a better predictor of reflection coefficient, and hence, increased central pulse pressure and decreased peripheral pulse flow, than either central pulse wave velocity alone or PWV gradient. The implication of this prediction is that, in clinical measurements of arterial stiffness, arterial diameter measurements should also be taken, if feasible. This analysis predicts that adverse cardiovascular events are associated, not only with arterial hardening, but also with arterial dimensional changes. Although the previous literature identifies arterial stiffness is a factor in arterial wave reflection and luminal area is also a factor, this analysis offers the unique combination of stiffnesses and luminal areas together, in each of the macrocirculation and mesocirculation, which are determinants in pulse wave reflection.

The finding that the value of area ratio of 1.26 in both the macrocirculation and the microcirculation (which is associated with a minimum in pulse wave reflection), is apparently identical to the value identified by Murray’s Law (which is associated with minimum work in moving steady flow through the arterial tree), was unexpected. The potential for these two minimized conditions being potentially physically identical is worthy of further fundamental research. In addition, the reservoir-wave analytic approach of Parker et al. [64–66], which is complementary to this impedance matching, wave-propagation approach, identifies the reservoir waveform as that associated with minimum work. The reservoir wave analytic approach includes an “excess waveform” component that identifies separate backward and forward waves. The physical relationships between the minimal pulse

wave reflection and minimal work and between the reservoir wave and impedance-matching wave propagation approaches also merit further basic research.

6 Study Limitations

This analysis of pulse wave reflections at arterial bifurcations, with their related pressure and flow linkages between the macrocirculation and microcirculation regions, is limited to the consideration of symmetric bifurcations. The results of the analysis are compared with the Womersley [10, 11] results, which were developed for symmetric bifurcations only. The human vasculature includes asymmetric junctions, including trifurcations and quadfurcations. The additional complexity of analyzing asymmetric bifurcations may obscure the physical and medical implications of the analysis. While analyses of impedance mismatch at asymmetric bifurcations have been reported [15, 22], such analyses draw on the Womersley approach involving the asymptotic expansion of Bessel functions which may also obscure the physical implications of the analysis. One consequence of the symmetric bifurcation assumption is that the resulting estimate of thirty generations of bifurcations between the aorta and the capillaries, as discussed in Sect. “4.8”, is probably an overestimation.

One basic purpose of the study was to extend Womersley’s seminal physics-based analysis of wave reflections at symmetric arterial bifurcations, to explicitly include arterial stiffnesses in both large and small arteries. The equations of reflection coefficient, (as a function of arterial stiffness and area ratios) developed in this analysis are closed form equations, which are relatively easily computed. The equations do not involve expansions of Bessel functions as provided in tabular form by Womersley.

The use of symmetric bifurcations in this analysis does not limit the generality of the principle which the analysis offers, that pulse wave reflections at arterial bifurcations are linked to both increased aortic pulse pressure and decreased peripheral pulse flow. The symmetric bifurcation focus also does not affect the principle that, with well matched arterial bifurcations, the central arteries are more compliant than the first few generations of branch arteries. For smaller arteries (less than about 3 mm diameter) however, the arteries soften, while the total arterial bed area increases with each generation of cascaded bifurcation.

The analysis and equations do not consider pulse wave reflections which may occur from arterial taper. The basic assumption of uniform wall thickness and stiffness in each arterial segment does not affect the pulse wave

reflection which occurs at arterial bifurcations. Although human arterial morphology has tapered arteries, mainly with a slowly decreasing luminal area, wave reflection is predicted to be a function of both luminal area and wall stiffness. Generally, arterial walls decrease in thickness with decreasing luminal area, thereby minimizing wave reflection in tapered arteries. In silico and phantom arterial models [67] indicate that the reflection site associated with arterial taper is distributed along the length of the arterial segment and is superimposed on reflections from individual major bifurcation sites.

In developing the closed form reflection coefficient Eqs. (44–48), linear approximations to the blood viscosity and the elastic modulus parameters were applied. These are the same linearization approximations used by Womersley [10, 11] and others [15, 22]. As discussed by Nichols [12], the impact of nonlinearities has been assessed [11, 68–70] to be relatively insignificant, particularly in relation to the potential for the nonlinearities giving rise to inter-modulation products of the Fourier harmonics of the heart rate.

With the occurrence of cyclically reversing flow, individual cells must stop and reverse direction at select arterial points. With the blood’s viscosity having a strong dependence on its flow velocity (at very low flow velocities the blood’s viscosity may be more than an order of magnitude greater than at normal systolic flow rates [71, 72]). Such viscosity non-linearity is anticipated to be significant in the narrower arteries in which the effect of viscosity is important. With arterial impedance in the macrocirculation being independent of viscosity (Eq. 29), the impact of flow velocity on macrocirculation impedance mismatch is predicted to be relatively minor, (as discussed by Nichols [12]). In the microcirculation, however, arterial impedance is dependent on the blood’s viscosity (through the dependence of impedance on Womersley’s number “ α ”, as identified in Eqs. (23) and (31)). The implication of an increase in viscosity would be an apparent decrease in the luminal area and the potential need for the introduction of a correction factor in the determination of optimum *Pulse Wave Velocity Ratio/Area Ratio* in the mesocirculation and microcirculation. With the focus of this analysis on the ratio of luminal areas, any flow velocity dependent correction factor which may be applied to the luminal area on both sides of a bifurcation is likely to be somewhat self-correcting in the determination of the equivalent luminal area ratio.

With the pulse wave’s amplitude attenuating as the wave propagates, the magnitude of the reverse flow component similarly decreases in progressing into

the microcirculation. Low and reversing flow velocities, with viscous dependence on flow velocity, will influence arteries' impedances and bifurcation wave reflections, particularly in the large reflection coefficient region of the mesocirculation. The current literature is relatively silent on pulsatile wave reflection in the mesocirculation, indicating the need for additional research related to wave reflection and flow reversal flow in this region of the vasculature. The potential impact of cyclically reversing flow on arterial wall shear stresses, with high blood viscosities, as associated with low flow rates, and the impact of such reversing flow on endothelial layer continuity and function, merits further clarification.

For arterioles (less than about 100 microns in diameter), the Fahraeus–Lindqvist [73, 74] effect will also affect blood viscosity. With relatively low pulsatility at such small arterial dimensions and the error-correcting effect which the ratio of luminal areas imparts, the applicability of the reflection coefficient Eqs. (44–48) for flow in the arterioles is indeterminate.

The analysis considers only the fundamental Fourier component of pulsatile waveforms. The reflection coefficient for each of the Fourier harmonic components of a pulsatile wave will display similar V-shaped plots (each as a function of Stiffness Ratio and Area Ratio) as displayed by the fundamental harmonic component, but for somewhat different arterial diameters. In the limits of the macrocirculation and the microcirculation the reflection coefficient, as described by Eqs. (33) and (42), are dependent only on Stiffness Ratio (SR) and Area Ratio (AR). Neither Stiffness Ratio nor Area Ratio, by their definitions, are dependent on frequency. However, the reflection coefficient in the mesocirculation is dependent on frequency, through the Womersley number (α). The Womersley number is dependent linearly on the arterial diameter and on the square root of the frequency. Hence, the first Fourier harmonic component (i.e., double the fundamental frequency) has the same reflection coefficient plot as the harmonic, but at a value of diameter that is $0.707 (2^{-1/2})$ of that of the fundamental frequency. The implication is that the luminal diameters which define the mesocirculation for the first Fourier harmonic are not 1–6 mm, but rather are 0.7–4.2 mm and for the second harmonic are 0.6 and 3.5 mm, etc. The practical implication of this is that the shape of the pulsatile wave will change slightly as it progresses through each bifurcation. The specific shape change will be dependent on the values of specific Fourier coefficients of the pulsatile waveform. However, in general, the shape of the pulse as it progresses through the mesocirculation into the microcirculation is predicted to become less

pulsatile (i.e., more sinusoidal at the fundamental frequency) and, with the low pass filtering of each bifurcation generation, also becomes reduced in amplitude.

7 Conclusions

This wave propagation-based analysis extends the seminal physics-based analyses offered by both Murray [31] in 1928 and by Womersley [11] in 1958. This analysis produces reflection coefficient plots for pulse waves introduced by impedance mismatches in flow through bifurcations of the macrocirculation, reflection coefficient plots which match Womersley's plots. The analysis predicts that in both the macrocirculation and microcirculation the optimum pulse wave antegrade flow conditions occur when the luminal areas of bifurcation trunk and branch arteries are as described by Murray's Scaling Law, but for specific values of arterial stiffness. For Murray's optimum area ratio value of 1.26 the optimum ratio of branch to trunk stiffness is 1.12 in the macrocirculation and 0.89 in the microcirculation. This analysis, therefore, offers a physics-based linkage between the classical analyses of Murray and Womersley. The analysis also predicts that if the luminal area ratio for a bifurcation does not satisfy Murray's Scaling Law, optimal antegrade pulse flow can still occur if the stiffness ratio for the bifurcation is adjusted to offset the nonoptimal area ratio.

The analysis predicts that the mesocirculation region, the region of the vasculature with arterial diameters between one and six millimeters, is the greatest pulse wave reflection region of the arterial tree, hence presents the greatest reduction to antegrade pulse wave flow. The optimum reflection coefficient predicted by this analysis is in the range 22–31%, which compares favourably with the value of clinically measured reflection factors of 30.9%, the averaged of 18 different studies, involving patients of all ages with various cardiovascular conditions.

Most of the current focus on arterial stiffness in hypertension relates to the aorta's stiffening with age and with cardiovascular diseases. This analysis indicates that any change in arterial stiffness or luminal area in any artery, either central or peripheral, which results in increased bifurcation impedance mismatch, can increase central and peripheral pulsatile pressure. Increased impedance mismatch also decreases pulse wave flow in downstream segments of the arterial tree, thereby influencing the perfusion of target organs. The analysis indicates that the recently proposed use of central to peripheral arterial stiffness gradient, as a predictor of adverse cardiovascular events, potentially offers sufficient improvement over currently used predictors to merit further research.

From the points of view of medical research and clinical practice, the predictions offered by this analysis

are potentially far reaching. The analysis predicts that increased pulse pressure which is a consequence of bifurcation impedance mismatch will affect both measures of pulse pressure amplification and augmentation index (as indicators of cardiovascular health). In various hypertensive conditions such as isolated systolic hypertension in youth, elevated brachial pulse pressure may be a consequence of pulse reflection from mesocirculation bifurcations for which the stiffness ratio is too low, rather than too high.

High flow demand organs, such as the heart, brain and kidneys are likely to be most affected by increased pulse wave reflection from mis-matched mesocirculation bifurcations. In chronic kidney disease, the Doppler measurement of the Pourcelot “Resistive” Index in the renal arteries provides some measure of renal pulse flow anomaly. However, the Pourcelot Index uses the maximum value of diastolic Doppler, indicative only of the maximum antegrade flow velocity at diastole. The impact of reversing flow (with accompanying increased blood viscosity) on endothelial function is not captured by the measurement of maximum antegrade diastolic flow. Given that reverse renal artery flow is profoundly symptomatic of end-stage renal disease, measurement of the maximum retrograde pulse flow in the renal arteries is required. This implies the need for a fundamental new Doppler ratio measure (using the existing Doppler ultrasound techniques) which is defined by the increment between maximum antegrade flow velocity and maximum retrograde flow velocity. This analysis indicates significant diagnostic value in greater clinical use of Doppler ultrasound measurements of the diastolic flow velocities into target organs, particularly in quantifying the amount of reverse or retrograde flow, with its associated blood viscosity increase and endothelial function decline. The measurement of brachial pulse pressure is not a measure of the pulse flow and perfusion of target organs.

Most current pharmaceutical treatments for hypertension in cardiovascular diseases are designed to reduce or control macrocirculation pressures, not mesocirculation elevated pulse pressures associated with pulse wave reflections. This analysis indicates the need for research on treatments which reduce central and peripheral pulse pressures through the minimization of pulse wave reflections from arterial bifurcations for which the arterial luminal areas and stiffnesses are not optimally matched.

Appendix A

Impedance Matching for Wave Propagation in a Compliant Vessel

Derivation of the Generalized Bifurcation Reflection Coefficient Equation

For pulsatile pressure waves propagating in a fluid-filled, compliant vessel the relationship between flow and pressure is determined by the vessel’s characteristic impedance (Z_C). The characteristic impedance is defined by the quotient of the wave’s pressure divided by its flow. The characteristic impedance is determined by [16, 19] the vessel’s longitudinal impedance (Z_L), and transverse impedance (Z_T), as given by Eq. (15):

$$\text{Characteristic Impedance : } Z_C = \sqrt{Z_L Z_T} \quad (15)$$

The longitudinal impedance, in turn, is related to the viscous resistance (R) to flow presented by the vessel’s walls and the inertial impedance (L) of the blood’s mass, as given by Eq. (16):

$$\text{Longitudinal Impedance : } Z_L = R + j\omega L \quad (16)$$

The transverse impedance (Z_T) is related to the stiffness, or its inverse, compliance, of the vessel (often described as capacitive impedance (C)), as given by Eq. (17):

$$\text{Transverse Impedance : } Z_T = \frac{1}{j\omega C} = -\frac{j}{\omega C} \quad (17)$$

In Eqs. (16) and (17), “ ω ” is the frequency of the heart rate, expressed in radians/sec and the “ j ” operator represents the out of phase (or orthogonal component) of the pressure wave relative to that of the flow, with $+j$ representing the pressure wave leading that of the flow wave and $-j$ representing the pressure wave’s phase lagging the flow wave. This analysis of pulsatile blood flow focuses on the pressure and flow relationships of the fundamental harmonic of the pulsatile wave, the largest amplitude harmonic, which is also the frequency of the heart rate. The three constituent components, “ R ”, “ L ” and “ C ”, which comprise the characteristic impedance, are given approximately by [16, 19] Eqs. (18)–(20):

$$R = \frac{8\mu}{\pi r^4}, \quad (18)$$

$$L = \frac{\rho}{\pi r^2}, \quad (19)$$

and

$$C = \frac{3\pi r^3}{2Eh} \tag{20}$$

In Eqs. (18)–(20), each of the constituent impedance components is dependent on the radius of the vessel “ r ”. In Eq. (18), the resistance to flow “ R ” also depends on the viscosity of the blood “ μ ”. In Eq. (19) the inertial component “ L ” also depends on the density of the blood “ ρ ”. In Eq. (20), the vessel wall’s compliant component “ C ” also depends on the vessel wall’s elastic modulus “ E ”, and thickness “ h ” (assumes $h < r$).

The impedance to flow, as a function of the three impedance components of “ R ”, “ L ” and “ C ”, is obtained by combining Eqs. (15)–(17), yielding Eq. (21):

$$Z_C = \left[\frac{L}{C} \right]^{\frac{1}{2}} \left[1 - \frac{jR}{\omega L} \right]^{\frac{1}{2}} \tag{21}$$

Substituting Eqs. (18)–(20) into Eq. (21) yields the relationship between the characteristic impedance and the vessel’s and the blood’s parameters, as given in Eq. (22):

$$Z_C = \left[\frac{2\rho Eh}{3r} \right]^{\frac{1}{2}} \left[1 - \frac{j8\mu}{\omega\rho r^2} \right]^{\frac{1}{2}} \left[\frac{1}{\pi r^2} \right] \tag{22}$$

Two parameters are defined, the Womersley [11] number, “ α ”, and a stiffness factor, “ S ”, as shown in Eqs. (23) and (24) respectively:

$$\alpha^2 \equiv \frac{\omega\rho r^2}{\mu} \tag{23}$$

and

$$S^2 \equiv \frac{2\rho Eh}{3} \tag{24}$$

The stiffness factor “ S ”, as defined here, includes the elastic modulus “ E ” of the vessel wall, the thickness “ h ” of the vessel wall, and the blood’s density “ ρ ”. This definition of arterial stiffness depends only on wall and blood material parameters and combines the effect of the vessel wall’s thickness and elasticity. Substituting Eqs. (23) and (24) into Eq. (22) results in a general equation for the characteristic impedance “ Z_C ” of the vessel, as a function of vessel wall stiffness “ S ”, luminal cross-sectional area “ A ”, luminal radius “ r ”, and Womersley number “ α ”, as given in Eq. (A11):

$$Z_C = \frac{S}{A\sqrt{r}} \left[1 - j\frac{8}{\alpha^2} \right]^{1/2} \tag{25}$$

where the cross-sectional area “ A ” of a cylindrical vessel is given by:

$$A = \pi r^2 \tag{26}$$

Although the above equations are based on the previously established analyses, the majority of the analysis below, and the associated plots, are fundamental and new developments.

The characteristic impedance of compliant vessels, as described [19] by Eq. (25), for arbitrarily large or small values of α , is solvable through application of the identity of Eq. (27):

$$\left[1 - \frac{j8}{\alpha^2} \right]^{\frac{1}{2}} = \frac{\left[\left[1 + \left[\frac{8}{\alpha^2} \right]^2 \right]^{\frac{1}{2}} + 1 \right]^{\frac{1}{2}}}{\sqrt{2}} - j \frac{\left[\left[1 + \left[\frac{8}{\alpha^2} \right]^2 \right]^{\frac{1}{2}} - 1 \right]^{\frac{1}{2}}}{\sqrt{2}} \tag{27}$$

Substituting Eq. (27) into Eq. (25) results in a generalized expression for the characteristic impedance of a compliant artery, as shown in Eq. (28):

$$Z_C = \frac{S}{A\sqrt{r}} \left[\left[\left[1 + \left[\frac{8}{\alpha^2} \right]^2 \right]^{\frac{1}{2}} + 1 \right]^{\frac{1}{2}} - j \left[\left[1 + \left[\frac{8}{\alpha^2} \right]^2 \right]^{\frac{1}{2}} - 1 \right]^{\frac{1}{2}} \right] \tag{28}$$

Equation (28) is simplified considerably in the two limiting cases of large arteries (diameter > 6 mm), and small arteries (diameter < 1 mm).

In the large artery case (diameter > 6 mm), the characteristic impedance of Eq. (28) is approximated by Eq. (29):

$$Z_C = \frac{S}{A\sqrt{r}} \tag{29}$$

In the small artery case (diameter < 1 mm), the characteristic impedance is approximated by Eq. (30):

$$Z_C = \frac{2S}{A\alpha\sqrt{r}} [1 - j] \tag{30}$$

In Eq. (30), the $[1 - j]$ term indicates a 45° phase difference between the pressure and the flow waves. The magnitude of the $[1 - j]$ term is $\sqrt{2}$, so the magnitude of the small artery’s characteristic impedance is given by Eq. (31):

$$|Z_C| = \frac{2\sqrt{2}S}{A\alpha\sqrt{r}} \tag{31}$$

Arterial bifurcations, in general, present abrupt changes to the artery’s characteristic impedance. Propagating pressure waves which impinge on changes in the characteristic impedance of the artery are partially reflected in retrograde wave flow. In the development of the wave reflection equation for the impedance mismatch which may occur at a bifurcation, a symmetrical

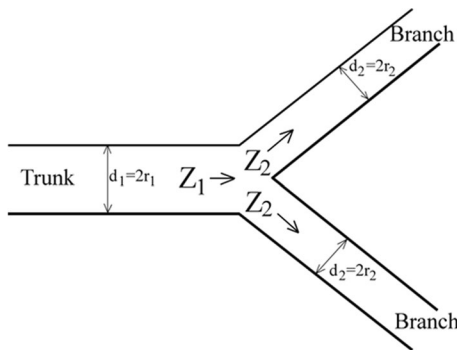


Fig. 7 Representation of a symmetric arterial bifurcation showing arterial dimensions and characteristic impedances (d =diameter, r =radius, Z =characteristic impedance, 1=trunk artery, 2=branch artery)

bifurcation is assumed, as shown in Fig. 7. The assumption of bifurcation symmetry is primarily to simplify the equations as an assist in reader interpretation of the results. Although in the human body a relatively small percentage of arterial junctions would normally be described as symmetric, in many junctions, particularly in the microcirculation which possesses the majority of the vascular bifurcations, asymmetry is relatively minor. The assumption of bifurcation symmetry in this analysis does not affect the validity of the physics principles affecting the cross-linkages between macrocirculation and microcirculation. References [15, 22] offer analyses of the impact of asymmetric bifurcations on pressure and flow in the macrocirculation.

Under the assumption that each branch artery is well matched at its distal end, the reflection coefficient “ RC ” associated with the bifurcation is determined by the ratio (or gradient) of characteristic impedances of the branch and trunk arteries, as given [15–20] by Eq. (32):

$$RC = \left| \frac{\left[\frac{Z_2}{2} - Z_1 \right]}{\left[\frac{Z_2}{2} + Z_1 \right]} \right| = \left| \frac{\left[\frac{Z_2}{2Z_1} - 1 \right]}{\left[\frac{Z_2}{2Z_1} + 1 \right]} \right| \quad (32)$$

where Z_1 is the characteristic impedance of the trunk artery and Z_2 is the impedance at the bifurcation of one of the branch arteries.

Under the condition that the branch artery is not well matched at its distal end, then the impedance at that distal end should be transformed along the length of the branch artery to the proximal (bifurcation) end. If the arteries are short in comparison to the inverse of the wave propagation’s attenuation coefficient and the impedance transformation is small. In this case the “effective” impedance [15, 44] of the branch artery approximates that of the

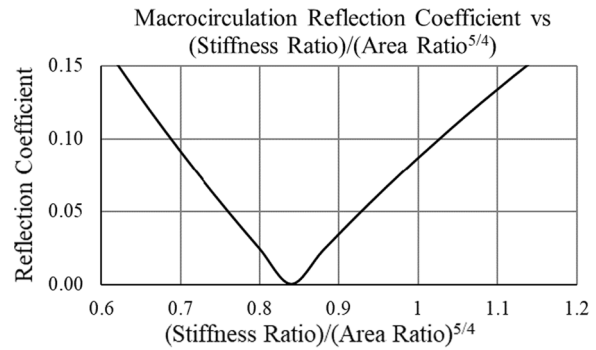


Fig. 8 Reflection Coefficient for a Large Artery (Macrocirculation) Bifurcation as a Function of the Bifurcation’s $(Stiffness\ Ratio)/(Area\ Ratio)^{5/4}$

sub-branches at the distal end of the branch artery (see Appendix C).

In the large artery (macrocirculation, $d > 6$ mm) case, by substituting the branch and trunk impedances of (Eq. 29) into Eq. (32), yields the relatively simple reflection coefficient Eq. (33):

$$RC = \left| \frac{\left[2^{1/4} SR [AR]^{-5/4} - 1 \right]}{\left[2^{1/4} SR [AR]^{-5/4} + 1 \right]} \right| \quad (33)$$

where SR is the ratio of arterial stiffnesses, branch-to-trunk, (which may also be called the stiffness gradient), as defined by Eq. (24), and as given by Eq. (34):

$$SR = \frac{S_2}{S_1} = \left[\frac{E_2 h_2}{E_1 h_1} \right]^{1/2} \quad (34)$$

In addition where AR is the branch-to-trunk luminal cross-sectional area ratio as defined by Eq. (35):

$$AR = \frac{2A_2}{A_1} = \frac{2r_2^2}{r_1^2} \quad (35)$$

A plot of Eq. (33), the reflection coefficient for a large artery bifurcation, as a function of the $(Stiffness\ Ratio)/(Area\ Ratio)^{5/4}$, is shown in Fig. 8. The macrocirculation’s bifurcation reflection coefficient plot of Fig. 8 shows that, for optimally matched bifurcations, there is negligible reflection under the specific condition that:

$$\begin{aligned} Stiffness\ Ratio &= 2^{-1/4} * Area\ Ratio^{5/4} \\ &= 0.841 * Area\ Ratio^{5/4}. \end{aligned} \quad (36)$$

If a matched macrocirculation bifurcation stiffness gradient (ratio) increases by 10%, in order that autonomic flow regulatory processes maintain a minimum in the reflection coefficient, and thereby maintain homeostasis in the branch arteries' pressures and flows, the bifurcation's area ratio must increase (vasodilate) by about 8%.

In the macrocirculation, if a bifurcation's area ratio is greater than about 1.15, then the stiffness ratio is greater than 1.0. for a well-matched bifurcation. In other words, for optimal match at a macrocirculation bifurcation, if the area ratio is greater than about 1.15, then the branch artery is predicted to be stiffer than the trunk artery.

For macrocirculation arteries the relationship between arterial stiffness, as defined here, and the more readily measurable pulse wave velocity (*PWV*) of a pressure wave, in a very thin-walled artery ($h < r$), is given by the Moens–Korteweg [12–17] Eq. (37):

$$PWV = \left[\frac{Eh}{2r\rho} \right]^{1/2} \quad (37)$$

For arteries in which the thin wall criteria of $h < r$ does not hold, the equation for pulse wave velocity becomes [12] Eq. (38):

$$PWV = \left[\frac{Eh}{2r\rho(1 - \sigma^2)} \right]^{1/2} \quad (38)$$

where σ is Poisson's ratio for the artery wall.

The pulse wave velocity ratio (*PWVR*), or gradient, for a bifurcation is defined by Eq. (39):

$$PWVR = \frac{PWV_2}{PWV_1} \quad (39)$$

Combining Eqs. (35, 37 and 39) results in the relationship between the stiffness ratio and the pulse wave velocity ratio as shown by Eq. (40):

$$PWVR = \frac{SR}{AR^{1/4}} \quad (40)$$

For large arteries, substituting (40) into (33) yields the bifurcation's branch-to-trunk reflection coefficient as shown by Eq. (41):

$$RC = \frac{\left[\frac{PWVR}{AR} - 1 \right]}{\left[\frac{PWVR}{AR} + 1 \right]} \quad (41)$$

A plot of the reflection coefficient as a function of [*Pulse Wave Velocity Ratio/Area Ratio*], applicable to the macrocirculation, is provided in Fig. 2 in the body of the text.

In the case of small arteries ($d < 1$ mm), the microcirculation case, the reflection coefficient assumes the relatively simple form of Eq. (42):

$$RC = \left| \frac{[SR [2^{3/4}] [AR]^{-7/4} - 1]}{[SR [2^{3/4}] [AR]^{-7/4} + 1]} \right| \quad (42)$$

A plot of Eq. (42), the reflection coefficient for a small artery bifurcation, as a function of the (*Stiffness Ratio*)/(*Area Ratio*)^{7/4}, is shown in Fig. 9.

The small artery (microcirculation) bifurcation reflection coefficient plot of Fig. 9 shows that, for matched microcirculation bifurcations, there is negligible reflection under the condition (Eq. 43) that:

$$\begin{aligned} \text{Stiffness Ratio} &= 2^{-3/4} * \text{Area Ratio}^{7/4} \\ &= 0.594 * \text{Area Ratio}^{7/4}. \end{aligned} \quad (43)$$

If the matched microcirculation bifurcation's stiffness ratio, increases by 10%, then for the autonomic flow regulatory processes to maintain a minimum in the reflection coefficient and thereby maintain homeostasis in peripheral pulse pressure and flow, Eq. (43) requires that the area ratio must increase, or vasodilate, by about 6%.

The circled area in Fig. 10, corresponds to the optimum conditions in which the stiffness ratio transitions from greater than unity in the macrocirculation to less than unity in the microcirculation. In youth the aorta is more compliant than its branch arteries. However, also in youth, in the smaller arteries, (i.e., the microcirculation) the branch arteries must be more compliant than their trunk arteries to ensure the arterioles are substantially more compliant than the more central arteries. The circled area is centered on a stiffness ratio of unity ($SR = 1.0$)

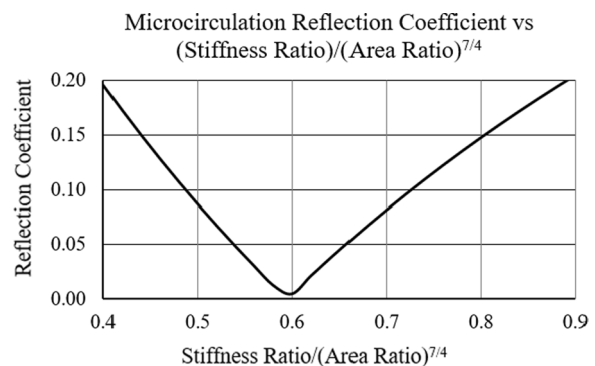


Fig. 9 Reflection Coefficient for a Small Artery (Microcirculation) Bifurcation, as a Function of (*Stiffness Ratio*)/(*Area Ratio*)^{7/4}

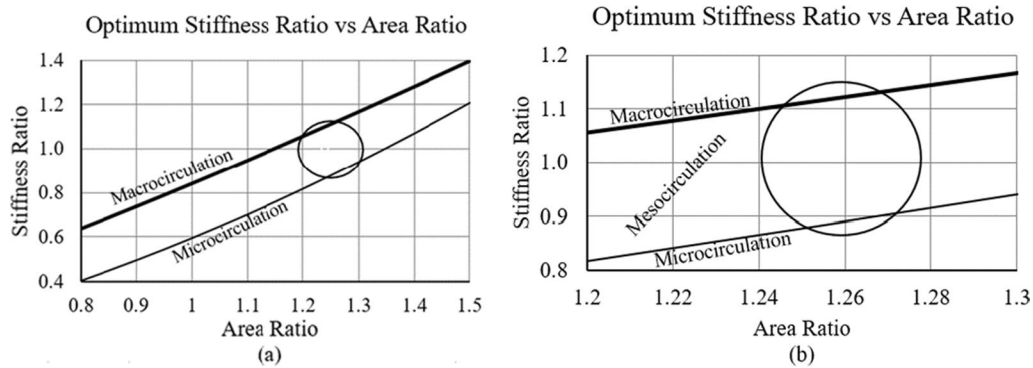


Fig. 10 **a** Optimum Stiffness Ratio as a function of Area Ratio for a minimum in bifurcation reflection coefficient for the two limiting cases of macrocirculation and microcirculation; **b** expanded plot of **(a)** with an optimum match in the centre of the mesocirculation region indicated

which corresponds to the arterial stiffness ratio in the mesocirculation transition from stiffer branch arteries to more compliant branch arteries. The area ratio which corresponds to a stiffness ratio of unity in the mesocirculation is in the range of about $AR=1.26-1.31$. The stiffness ratio in both the macrocirculation and microcirculation which corresponds to the optimum match is also approximately $AR=1.26$.

The stiffness ratio in the macrocirculation which corresponds to $AR=1.26$, is approximately $SR=1.12$. In other words, in the macrocirculation, for which arterial diameters are greater than about 6 mm, the arteries become stiffer (in youth) in progressing from the aorta into its branch arteries.

However, in the microcirculation the stiffness ratio which corresponds to $AR=1.26$ is about $SR=0.89$. In other words, in the microcirculation in proceeding from generation to generation of cascaded bifurcations, the area ratio increases while the stiffness ratio decreases.

An area ratio of 1.26 corresponds to the diameter of each bifurcation branch being approximately 79% of that of its trunk artery. In other words, in the microcirculation, at each level, or generation, in a progression of cascaded bifurcations, while the diameter of individual branch arteries reduces, the stiffness of those arteries simultaneously also reduces. Hence, in the microcirculation, the analysis predicts that, while the total cross-sectional area of the arterioles and capillaries may be substantially greater than that of the central arteries, they may also, simultaneously, be substantially more compliant.

The equation for the generalized reflection coefficient for a symmetric bifurcation, applicable to all values of Womersley number (i.e., all arterial diameters), is given by Eqs. (44–48):

$$RC = \frac{[2^{1/4}a(SR)AR^{-5/4} - c] + j[2^{1/4}b(SR)AR^{-5/4} - d]}{[2^{1/4}a(SR)AR^{-5/4} + c] - j[2^{1/4}b(SR)AR^{-5/4} + d]} \tag{44}$$

where:

$$a \equiv \frac{\left[\left[1 + \left[\frac{16}{AR*\alpha_1^2} \right]^2 \right]^{\frac{1}{2}} + 1 \right]^{\frac{1}{2}}}{\sqrt{2}} \tag{45}$$

$$b \equiv \frac{\left[\left[1 + \left[\frac{16}{AR*\alpha_1^2} \right]^2 \right]^{\frac{1}{2}} - 1 \right]^{\frac{1}{2}}}{\sqrt{2}} \tag{46}$$

$$c \equiv \frac{\left[\left[1 + \left[\frac{8}{\alpha_1^2} \right]^2 \right]^{\frac{1}{2}} + 1 \right]^{\frac{1}{2}}}{\sqrt{2}} \tag{47}$$

$$d \equiv \frac{\left[\left[1 + \left[\frac{8}{\alpha_1^2} \right]^2 \right]^{\frac{1}{2}} - 1 \right]^{\frac{1}{2}}}{\sqrt{2}} \tag{48}$$

Equations (44) through (48) provide a general solution for pulsatile wave reflection at bifurcations, and is applicable in all arterial segments, including the mesocirculation segment (i.e., for all combination of stiffness and area ratios).

Figure 11 shows plots of reflection coefficient for bifurcations, (as a function of Area Ratio and Stiffness Ratio) for four different values of arterial diameter (including: (a) the macrocirculation; (b) and (c) the mesocirculation; and (d) the microcirculation) and for three different values of branch-to-trunk stiffness ratio ($SR=1.1$, $SR=1.0$

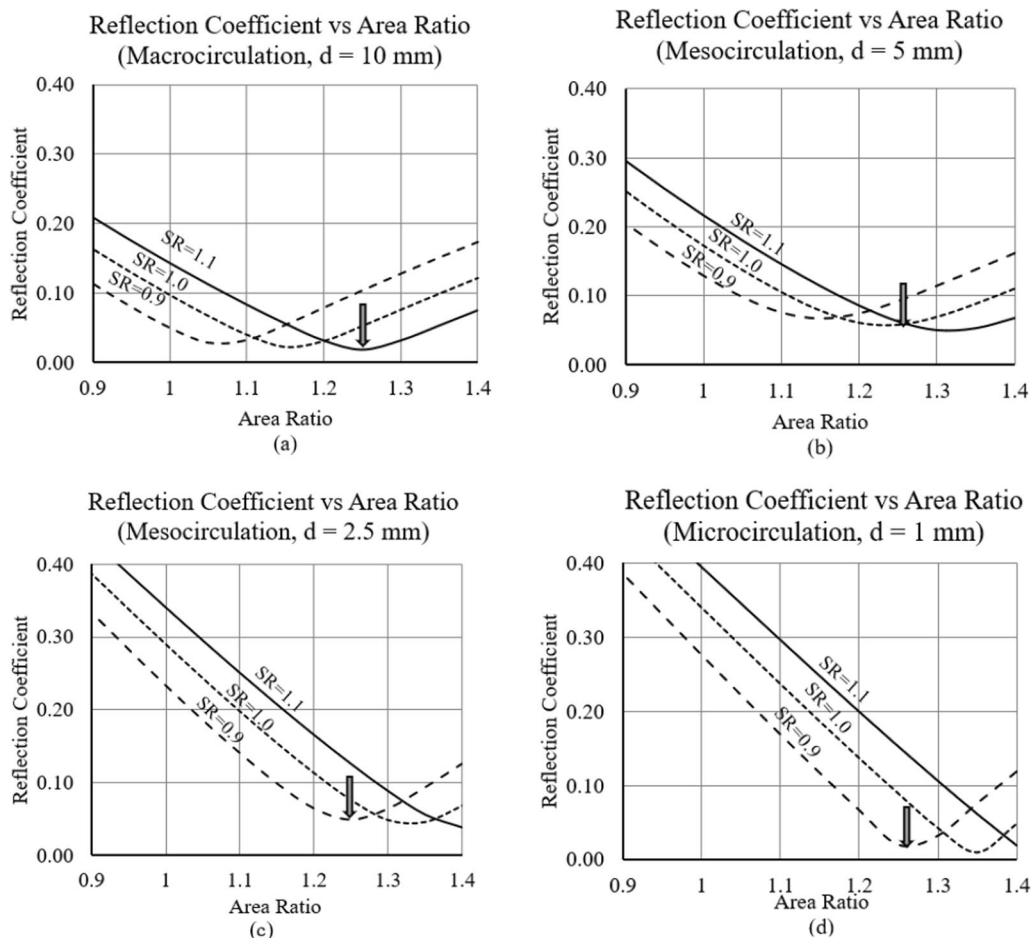


Fig. 11 Plots of Reflection Coefficient as a function of Area Ratio for four different values of trunk artery diameter (**a** $\alpha=8$, trunk diameter = 10 mm. **b** $\alpha=4$, trunk diameter = 5 mm. **c** $\alpha=2$, trunk diameter = 2.5 mm. **d** $\alpha=0.8$, trunk diameter = 1 mm. In each of the four graphs above there are three different plots of stiffness ratio shown: (SR = 1.1—solid line; SR = 1.0—short dashes; SR = 0.9—long dashes). The arrows indicate the point at which area ratio $AR=1.26$

and $SR=0.9$). The arrows in Fig. 11 indicate the stiffness match corresponding to an area ratio of approximately 1.26 for each of the four arterial diameters shown.

The minimum in the reflection coefficient plots (corresponding to the optimum impedance match) predicted for bifurcations in the mesocirculation, the transition region between the macrocirculation and the microcirculation, as indicated in Fig. 11c and d, lies typically in the range of 4–6%. Compared with the minimum, or optimum, reflection coefficient predicted for bifurcations in both the microcirculation and macrocirculation (which are near zero) the predicted (relatively large value of reflection coefficient in the transition region) represents a potentially significant contribution to the total reflection coefficient associated with the extended arterial tree.

Appendix B

Definitions of Macrocirculation, Microcirculation and Mesocirculation

Standardized definitions of macrocirculation and microcirculation are somewhat elusive [75]. For the purposes of this analysis, microcirculation arteries are defined as those whose diameters are less than 1000 microns ($d < 1.0$ mm). Arteries of the macrocirculation are defined as those whose diameters are greater than 6000 microns ($d > 6.0$ mm). In addition, a transitional circulatory region between the macrocirculation and the microcirculation, described here as the mesocirculation, applies to arteries that are between 1.0 and 6.0 mm in diameter.

The reason for selecting these specific circulation boundary values is demonstrated in the plots of Fig. 12. With a major focus of this analysis of bifurcation reflection coefficients, if the arterial diameter is less than about 1.0 mm, then the reflection coefficient plot is

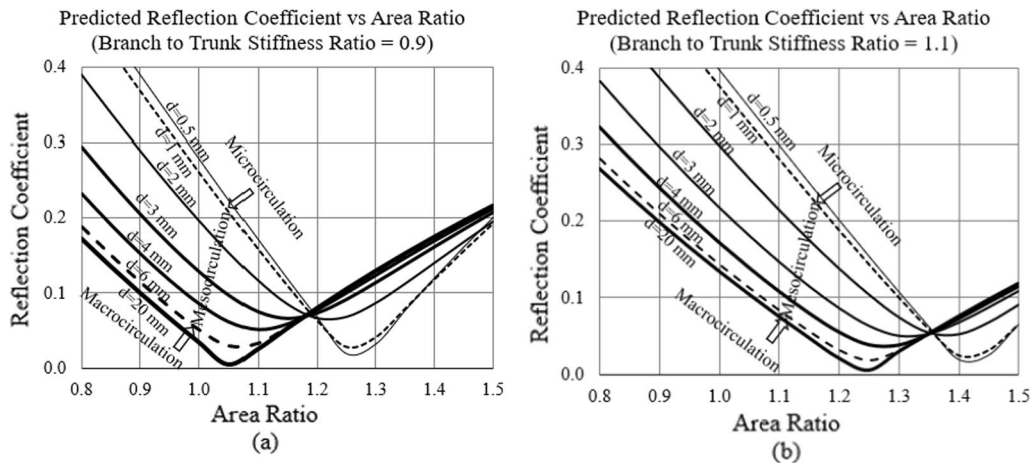


Fig. 12 Plots of reflection coefficient, as a function of branch to trunk area ratios for six arterial diameters **a** branch to trunk stiffness ratio = 0.9 (i.e., the branch artery are softer than the trunk artery, and **b** branch to trunk stiffness ratio = 1.1 (i.e., the branch arteries are stiffer than the trunk)

independent of the absolute value of arterial diameter and the minimum (optimum) reflection coefficient is close to zero. For these small diameter microcirculation arteries, the impedance is dominated by viscous resistance.

On the other hand, if the arterial diameter is greater than about 6 mm the reflection coefficient plot is again independent of the absolute value of the diameter, and the optimum (minimum) reflection coefficient is close to zero. In this large artery macrocirculation case, the viscous resistance is negligible, and the reflection coefficient is dominated by the balance between the compliant response of the arterial wall and the inertial response of the stroke (or mass) of blood in the artery.

A macrocirculation artery of 20 mm diameter, (as plotted in Fig. 12a and b) is comparable to the abdominal aorta. An artery of 6 mm diameter, which represents the smallest macrocirculation artery and, also represents the beginning of the mesocirculation, is comparable to the

femoral, brachial, and internal carotid arteries. An artery of 1 mm diameter, which represents the largest of the microcirculation arteries, is comparable to many small arteries such the ophthalmic artery.

For the case in which branch arteries are stiffer than trunk arteries, as is the case in youth and good health, for central bifurcations (such as the macrocirculation’s aortic/iliac bifurcation), with the plots of Fig. 12b representative of branch arteries stiffer than trunk arteries (SR = 1.1), the optimum area ratio is about 1.26. In the macrocirculation the minimum reflection coefficient is close to zero

For the case in which the branch arteries are softer than the trunk arteries, as occurs in the continuous softening of arteries in progressing through the cascaded generations of bifurcations of the microcirculation, for a stiffness ratio of 0.9 the optimum area ratio is also about 1.26 (see Fig. 12a). In the microcirculation the minimum reflection coefficient is also close to zero.

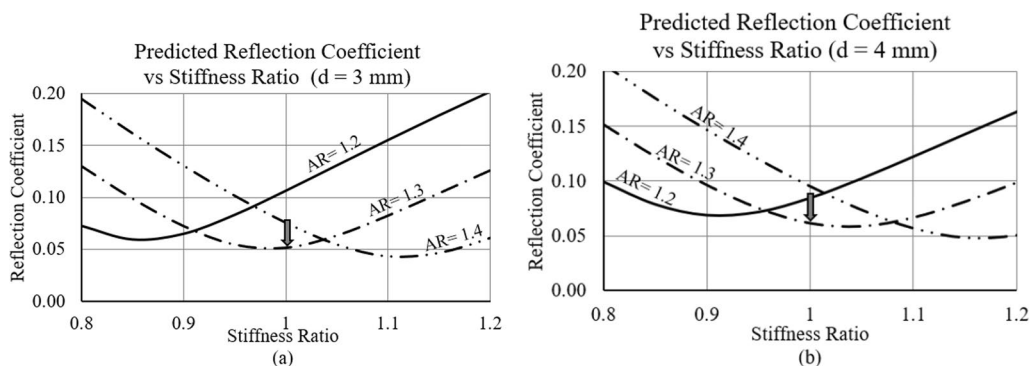


Fig. 13 Plots of Reflection Coefficient as a function of branch to trunk stiffness ratio for various values of branch to trunk area ratio for two different trunk arterial diameters in the mesocirculation region **a** trunk diameter = 3 mm, and **b** trunk diameter = 4 mm.)

In the mesocirculation (arterial diameters between 1.0 and 6.0 mm) the minimum reflection coefficient, is finite, in the range of, typically 4–6%, (as shown in Fig. 13), as contrasted with the low values of minimum reflection coefficient for optimally matched bifurcations of the macrocirculation and microcirculation. The optimum area ratio in the mesocirculation varies with arterial diameter. In the middle of the mesocirculation region, assuming equal arterial stiffnesses on either side of the bifurcation (arrows in Fig. 13 at SR=1.0) the optimum area ratio is about 1.3, slightly greater than that in the microcirculation and macrocirculation. Of fundamental importance is that the minimum in reflection coefficient for the bifurcations in the middle of the mesocirculation region is not near zero, but rather about 4–6%, representing the most significant individual contributors to reflection in a wave's propagation through cascaded generations of bifurcations.

Appendix C

Estimation of Optimum Aggregate Mesocirculation Reflection Coefficient

The minimum reflection coefficient for bifurcations in the macrocirculation is near zero if the characteristic impedances on either side of the bifurcation are equal and if the load impedances at the distal end of each of the bifurcation's branches is matched to the characteristic impedance of each branch (i.e., if the branch is well matched to its sub-branches). If, however, the branch is mis-matched at its distal end, then that mismatch (with its reflection coefficient RC_{2mis}) is transformed along the branch to its proximal end at the bifurcation. This sub-branch reflection transforms the branches' impedances at the bifurcation, from the characteristic Z_2 to a value of Z_{2mis} as given [65, 66, 76] by Eq. (49):

$$Z_{2(mis)} = Z_2 * [1 + RC_{2mis}] / [1 - RC_{2mis}] \quad (49)$$

where Eq. (49) assumes that the length of the branch is sufficiently short that the wave is not appreciably attenuated in transit along the branch's length. The attenuation coefficient of each artery is a function of the artery's diameter. Reported [72] measured values of attenuation coefficient (σ) for various arteries are as follows: $\sigma_{AbdominalAorta} = 0.5 \text{ m}^{-1}$, $\sigma_{Iliac} = 1.0 \text{ m}^{-1}$, $\sigma_{Femoral} = 1.7 \text{ m}^{-1}$, and $\sigma_{Carotid} = 1.2 \text{ m}^{-1}$. For artery lengths that are small relative to the reciprocal of the attenuation coefficient, the assumption is valid.

In the center of the mesocirculation region the optimum (minimum) value of RC_{2mis} is about 4–6% which implies that Z_{2mis} can be approximated by Eq. (50):

$$Z_{2mis} \approx Z_2 * [1 + 2RC_{2mis}] \quad (50)$$

The impedance of each branch artery is, therefore, increased by a factor of $[1 + 2RC_{2mis}]$ which affects the reflection coefficient (see Eq. 15) at the trunk-to-branch bifurcation as shown in Eq. (51):

$$RC = \left| \frac{\left[\frac{Z_{2mis}}{2Z_1} - 1 \right]}{\left[\frac{Z_{2mis}}{2Z_1} + 1 \right]} \right| \quad (51)$$

Substituting Eq. (50) into (51) results in Eq. (52):

$$RC = \left| \frac{\left[\frac{Z_2[1+2RC_{2mis}]}{2Z_1} - 1 \right]}{\left[\frac{Z_2[1+2RC_{2mis}]}{2Z_1} + 1 \right]} \right| \quad (52)$$

Under the assumption that the characteristic impedances of the trunk and its branches are, themselves well matched (i.e., $Z_2/2Z_1 \approx 1$) then the value of the reflection coefficient for the trunk-to-branch bifurcation is given by Eq. (53):

$$RC \approx RC_{2mis} \quad (53)$$

To a first order of approximation, therefore, the mismatch at the distal end of a mesocirculation branch artery is transferred to mismatch the primary trunk-to-branch bifurcation.

Figures 4 and 13 (Appendix B) indicate that near the centre of the mesocirculation, which corresponds to an arterial diameter of about 3 mm, the optimum reflection coefficient for that centre bifurcation of the mesocirculation is in the range of 4–6%. With 8 bifurcations in the mesocirculation, to attain the maximum reflection coefficient of 4% in the centre of mesocirculation, through about four generations of bifurcations, implies each successive bifurcation increments the reflection by about 1%. With each branch in the mesocirculation sequentially mismatched by increments of 1%, the total mismatch, corresponding to minimum aggregate reflection coefficient, is estimated to be about 21.7% ($1.01 * 1.02 * 1.03 * 1.04 * 1.04 * 1.03 * 1.02 * 1.01 = 1.217$). Hence, even in youth, with assumed optimum arterial impedance matching, there is predicted to be finite and significant wave reflection in the macrocirculation caused by essential mismatches in the mesocirculation.

This analysis indicates that an optimally designed mesocirculation bifurcation presents an inherent impedance mismatch with finite wave reflection into the macrocirculation, and with an attendant central pulse pressure increase.

Author contributions

A single author only.

Funding

Self funded. No outside funding to declare.

Availability of data and materials

Analysis software available on request.

Declarations**Conflict of interest**

No competing or conflicting interest exist.

Ethics approval and consent to participate

None required.

Consent for publication

Consent is hereby provided for publication.

Received: 6 March 2023 Accepted: 9 May 2023

Published online: 28 May 2023

References

- O'Rourke MF, Hashimoto J. Mechanical factors in arterial aging: a clinical perspective. *J Am Coll Cardiol.* 2007;50(1):1–13. <https://doi.org/10.1016/j.jacc.2006.12.050>.
- Struijckera-Boudier HAJ, Cohuet G, Baumann M, Safar ME. The heart, macrocirculation and microcirculation in hypertension: a unifying hypothesis. *J Hypertension.* 2003;21(Suppl3):S19–23.
- Safar ME, Lacolley P. Disturbance of macro- and microcirculation: relations with pulse pressure and cardiac organ damage. *Am J Physiol Heart Circ Physiol.* 2007;293:H1–7. <https://doi.org/10.1152/ajpheart.00063.2007>.
- Laurent S, Briet M, Boutouyrie P. Large and small artery cross-talk and recent morbidity-mortality trials in hypertension. *Hypertension.* 2009;54:388–92. <https://doi.org/10.1161/hypertensionaha.109.133116>.
- Feihl F, Liaudet L, Waeber B. The macrocirculation and microcirculation of hypertension. *Curr Sci.* 2009;11:182–9. <https://doi.org/10.1007/s11906-009-0033-6>.
- Laurent S, Boutouyrie P. The structural factor of hypertension: large and small artery alterations. *Circ Res.* 2015;116:1007–21. <https://doi.org/10.1161/circresaha.116.303596>.
- Rizzoni D, De Ciuceis C, Salvetti M, Paini A, Rossini C, Agabiti-Rosei C, Lorenza MM. Interactions between macro- and micro-circulation: are they relevant? *High Blood Press Cardiovasc Prev.* 2015;22:119–28. <https://doi.org/10.1007/s40292-015-0086-3>.
- Laurent S, Agabiti-Rosei C, Bruno RM, Rizzoni D. Microcirculation and macrocirculation in hypertension: a dangerous cross-link? *Hypertension.* 2022;79:479–90. <https://doi.org/10.1161/hypertensionaha.121.17962>.
- Kondiboyina A, Harrington HA, Smolich JJ, Cheung MMH, Mynard JP (2022) optimised design of an arterial network model reproduces characteristic central and peripheral hemodynamic waveform features in young adults. Preprints 2022030230. <https://doi.org/10.20944/preprints202203.0230.v1>
- Womersley JR. Method for the calculation of velocity, rate of flow and viscous drag in arteries when the pressure gradient is known. *J Physiol.* 1955;127:553–63.
- Womersley JR. Oscillatory flow in arteries II: the reflection of the pulse wave at junctions and rigid inserts in the arterial system. *Phys Med Biol.* 1958;2:313–23.
- Nichols W, O'Rourke M, Vlachopoulos C (2011) McDonald's blood flow in arteries—theoretical, experimental and clinical principles, 6th edn. CRC Press, Boca Raton. ISBN 13: 978-1-4441-2878-9
- Noordergraaf A (2011) Blood in motion. Springer, New York. ISBN 9781461400059
- Caro CG, Pedley TJ, Schroter RC, Seed WA (2012) The mechanics of the circulation, 2nd edn. Cambridge University Press, UK. ISBN 978-0-521-15177-1
- Zamir M (2016) Hemo-dynamics. Springer International, Switzerland. ISBN 978-3-319-24101-2. <https://doi.org/10.1007/978-3-319-24103-6>
- Westerhof N, Stergiopulos N, Noble M, Westerhof B (2019) Snapshots of hemodynamics—an aid for clinical research and graduate education, 3rd edn. Springer Nature, Switzerland. ISBN 978-3-319-91931-7. <https://doi.org/10.1007/978-3-319-91932-4>
- Chirinos JA (2022) Textbook of arterial stiffness and pulsatile hemodynamics in health and disease. Editor, Academic Press, London. ISBN: 9780323913911
- Segers P, Chirinos JA (2022) Essential principles of pulsatile pressure-flow relations in the arterial tree. In: Chirinos JA (ed) Textbook of arterial stiffness and pulsatile hemodynamics in health and disease, vol 1, Chapter 3. Academic Press, London. ISBN: 9780323913911
- Tucker T. Arterial stiffness as a vascular contribution to cognitive impairment: a fluid dynamics perspective. *Biomed Phys Eng Express.* 2021;7:025016. <https://doi.org/10.1088/2057-1976/abdf36>.
- Tucker T (2022) A fluid dynamics perspective of arterial stiffness in arteriosclerotic development. In: Bennington EH (ed) Horizons in cardiovascular research, vol 23, Ch3, pp 99–195. ISBN 978-1-53616-925-6
- Greenwald SE, Carter AC, Berry CL. Effect of age on the in vitro reflection coefficient of the aortoiliac bifurcation in humans. *Circulation.* 1990;82:114–23. <https://doi.org/10.1161/01.circulationaha.82.1.114>.
- Brown N. Impedance matching at arterial bifurcations. *J Biomechanics.* 1993;26(1):59–67. [https://doi.org/10.1016/0021-9290\(93\)90613-j](https://doi.org/10.1016/0021-9290(93)90613-j).
- Lighthill MJ. Physiological fluid dynamics: a survey. *J Fluid Mech.* 1972;52(3):475–97. <https://doi.org/10.1017/S0022112072001557>.
- Sherman TF. On connecting large vessels to small. The meaning of Murray's Law. *J Gen Physiol.* 1981;79:431–53.
- Wu S, Chen D, Zeng X, Wen J, Zhou C, Xiao K, Hu P, Chen W. Arterial stiffness is associated with target organ damage in subjects with pre-hypertension. *Arch Med Sci.* 2018;14(6):1374–80. <https://doi.org/10.5114/aoms.2017.69240>.
- Mitchell GF. Aortic stiffness, pressure and flow pulsatility, and target organ damage. *J Appl Physiol.* 2018;125:1871–80. <https://doi.org/10.1152/japplphysiol.00108.2018>.
- Vasan RS, Short MI, Niiranen TJ, Xanthakis V, DeCarli C, Cheng S, Seshadri S, Mitchell GF. Interrelations between arterial stiffness, target organ damage, and cardiovascular disease outcomes. *J Am Heart Assoc.* 2019;8:e012141. <https://doi.org/10.1161/jaha.119.01214>.
- Pollack GH, Reddy RV, Noordergraaf A. Input impedance, wave travel, and reflections in the human pulmonary arterial tree: studies using an electrical analog. *IEEE Trans Biomed Eng.* 1968;15(3):151–64. <https://doi.org/10.1109/TBME.1968.4502559>.
- Hainsworth R. The importance of vascular capacitance in cardiovascular control. *Physiology.* 1990;5(6):250–4. <https://doi.org/10.1152/physiologyonline.1990.5.6.250>.
- Gelman S. Venous function and central venous pressure: a physiologic story. *Anesthesiology.* 2008;108:735–48. <https://doi.org/10.1097/aln.0b013e3181672607>.
- Murray CD. The physiological principle of minimum work: I. The vascular system and the cost of blood volume. *Biological Sci.* 1926;12(3):207–14. <https://doi.org/10.1073/pnas.12.3.207>.
- Huo Y, Kassab GS. A scaling law of vascular volume. *Biophys J.* 2009;96:347–53. <https://doi.org/10.1016/j.bpj.2008.09.039>.
- Finet G, Gilard M, Perrenot B, Rioufol G, Motreff P, Gavitt L, Prost R. Fractal geometry of arterial coronary bifurcations: a quantitative coronary angiography and intravascular ultrasound analysis. *EuroIntervention.* 2008;3(4):490–8. <https://doi.org/10.4244/eijv3i4a87>.
- Yamamoto T, Ogasawara Y, Kimura A, Tanaka H, Hiramatsu O, Tsujioka K, Lever J, Parker KH, Jones C, Caro CG, Kajiya F. Blood velocity profiles in the human renal artery by doppler ultrasound and their relationship to atherosclerosis. *Arterioscler Thromb Vase Biol.* 1996;16:172–7. <https://doi.org/10.1161/01.ATV.16.1.172>.
- Mitchell GF, Lacourcière Y, Ouellet JP, Izzo JL Jr, Neutel J, Kerwin LJ, Block AJ, Pfeffer MA. Determinants of elevated pulse pressure in middle-aged and older subjects with uncomplicated systolic hypertension—the role of proximal aortic diameter and the aortic pressure-flow relationship.

- Circulation. 2003;108:1592–8. <https://doi.org/10.1161/01.cir.0000093435.04334.1f.g>.
36. Mitchell GF, Wang N, Palmisano JN, Larson MG, Hamburg NM, Vita JA, Levy D, Benjamin EJ, Vasan RS. Hemodynamic correlates of blood pressure across the adult age spectrum noninvasive evaluation in the Framingham Heart Study. *Circulation*. 2010;122:1379–86. <https://doi.org/10.1161/circulationaha.109.914507>.
 37. Hashimoto J, Ito S. Pulse pressure amplification, arterial stiffness, and peripheral wave reflection determine pulsatile flow waveform of the femoral artery. *Hypertension*. 2010;56:926–33. <https://doi.org/10.1161/hypertensionaha.110.159368>.
 38. Hashimoto J, Ito S. Central pulse pressure and aortic stiffness determine renal hemodynamics—pathophysiological implication for microalbuminuria in hypertension. *Hypertension*. 2011;58:839–46. <https://doi.org/10.1161/hypertensionaha.111.177469>.
 39. Mitchell GA, Buchem MA, Sigurdsson S, Gotal JD, Jonsdottir MK, Ólafur Kjartansson O, Melissa Garcia M, Aspelund T, Harris TB, Gudnason V, Launer LJ. Arterial stiffness, pressure and flow pulsatility and brain structure and function: the Age, Gene/Environment Susceptibility—Reykjavik Study. *Brain*. 2011;134(11):3398–407. <https://doi.org/10.1093/brain/awr253>.
 40. Hashimoto J, Ito S. Aortic stiffness determines diastolic blood flow reversal in the descending thoracic aorta: potential implication for retrograde embolic stroke in hypertension. *Hypertension*. 2013;62:542–9. <https://doi.org/10.1161/hypertensionaha.113.01318>.
 41. Coutinho T, Borlaug BA, Pellikka PA, Turner ST, Kullo IJ. Sex differences in arterial stiffness and ventricular-arterial interactions. *JACC*. 2013;61(1):96–103. <https://doi.org/10.1161/hypertensionaha.120.16249>.
 42. Bensalah MZ, Bollache E, Kachenoura N, Giron A, De Cesare A, Macron L, Lefort M, Redheuil A, Mousseaux E. Geometry is a major determinant of flow reversal in proximal aorta. *Am J Physiol Heart Circ Physiol*. 2014;306:H1408–16. <https://doi.org/10.1152/ajpheart.00647.2013>.
 43. Torjesen AA, Wang N, Larson MG, Hamburg NM, Vita JA, Levy D, Benjamin EJ, Vasan RS, Mitchell GF. Forward and backward wave morphology and central pressure augmentation in men and women in the Framingham Heart Study. *Hypertension*. 2014;64:259–65. <https://doi.org/10.1161/hypertensionaha.114.03371>.
 44. Hashimoto JH, Ito S. Aortic blood flow reversal determines renal function potential explanation for renal dysfunction caused by aortic stiffening in hypertension. *Hypertension*. 2015;66:61–7. <https://doi.org/10.1161/hypertensionaha/115.05236>.
 45. Bretón-Romero R, Wan N, Palmisano J, Larson MG, Vasan RS, Mitchell GF, Benjamin EJ, Vita JA, Hamburg NM. Cross-sectional associations of flow reversal, vascular function, and arterial stiffness in the Framingham Heart Study. *Arterioscler Thromb Vase Biol*. 2016;36(12):2452–9. <https://doi.org/10.1161/ATVBAHA.116.307948>.
 46. Kim MO, Li Y, Wei F, Wang J, O'Rourke MF, Adji A, Avolio AP. Normal cerebral vascular pulsations in humans: changes with age and implications for microvascular disease. *J Hypertension*. 2017;35(11):2245–56. <https://doi.org/10.1097/HJH.0000000000001459>.
 47. Jue J, Boodhwani M, Beauchesne L, Dennie C, Nagpal S, Chan KL, Coutinho T. Greater aortic stiffness and pulsatile arterial load are associated with larger thoracic aortic aneurysm size in women. *Circulation*. 2019;139:1124–6. <https://doi.org/10.1161/circulationaha.118.037630>.
 48. London GM, Pannier B, Safar ME. Arterial stiffness gradient, systemic reflection coefficient, and pulsatile pressure wave transmission in essential hypertension. *Hypertension*. 2019;74:1366–72. <https://doi.org/10.1161/hypertensionaha.119.13387>.
 49. Evdochim L, Zhdanov AE, Borisov VI, Dobrescu D. Reflection coefficient in pressure pulse of human blood flow. In: 13th Int IEEE Conf on Comm (COMM). 18–20 June 2020. Bucharest, Romania. <https://doi.org/10.1109/comm48946.2020.9142027.49>
 50. Jarvis K, Soulat G, Scott M, Vali A, Pathrose A, Syed AA, Kinno M, Prabhakaran S, Collins JD, Markl M. Investigation of aortic wall thickness, stiffness and flow reversal in patients with cryptogenic stroke: a 4D flow MRI study. *J Magn Reson Imaging*. 2021;53:942–52. <https://doi.org/10.1002/jmri.27345>.
 51. Haidar MA, van Buchem MA, Sigurdsson S, Gotal JB, Gudnason V, Launer LJ, Mitchell GF. Wave reflection at the origin of a first-generation branch artery and target organ protection, the AGES-Reykjavik Study. *Hypertension*. 2021;77:1169–77. <https://doi.org/10.1161/hypertensionaha.120.16696>.
 52. Hashimoto J, Tagawa K, Westerhof BE, Ito S. Central-to-peripheral stiffness gradients determine diastolic pressure and flow fluctuation waveforms: time domain analysis of femoral artery pulse. *J Hypertension*. 2022;40:338–47. <https://doi.org/10.1097/hjh.0000000000003014>.
 53. Laurent S, Cockcroft J, Van Bortel L, Boutouyrie P, Giannattasio C, Hayoz D, Pannier B, Vlachopoulos C, Wilkinson I, Struijker-Boudier H. Expert consensus document on arterial stiffness: methodological issues and clinical applications. *Europe Heart J*. 2006;27:2588–605. <https://doi.org/10.1093/eurheartj/ehl254>.
 54. Van Bortel LM, Laurent S, Boutouyrie P, Chowienczyk P, Cruickshank JK, De Backer T, Filipovsky J, Huybrechts S, Mattace-Raso FUS, Protogerou AD, Schillaci G, Segers P, Vermeersch S, Weber T. Expert consensus document on the measurement of aortic stiffness in daily practice using carotid-femoral pulse wave velocity. *J Hypertens*. 2012;30:445–8. <https://doi.org/10.1097/hjh.0b013e32834fa8b0>.
 55. Townsend RR, Wilkinson IB, Schiffrin EL, Avolio AP, Chirinos JA, Cockcroft JR, Heffernan KS, Lakatta EG, McEniery CM, Mitchell GF, Najjar SS, Nichols WW, Urbina EM, Weber T. Recommendations for improving and standardizing vascular research on arterial stiffness: a scientific statement from the American Heart Association. *Hypertension*. 2015;66:698–722. <https://doi.org/10.1161/hyp.0000000000000033>.
 56. Safar ME, Asmar R, Benetos A, Blacher J, Boutouyrie P, Lacolley P, Laurent S, London G, Pannier B, Protogerou A, Regnault V. Interaction between hypertension and arterial stiffness: an expert reappraisal. *Hypertension*. 2018;72:796–805. <https://doi.org/10.1161/hypertensionaha.118.11212>.
 57. London GD. Arterial stiffness in chronic kidney disease and end-stage renal disease. *Blood Purif*. 2018;45:154–8. <https://doi.org/10.1159/000485146>.
 58. Nagayama D, Fujishiro K, Miyoshi T, Horinaka S, Suzuki K, Shimizu K, Saiki A, Shirai K. Predictive ability of arterial stiffness parameters for renal function decline: a retrospective cohort study comparing cardio-ankle vascular index, pulse wave velocity and cardio-ankle vascular index. *J Hypertens*. 2022;40:1294–302. <https://doi.org/10.1097/hjh.00000000000003137>.
 59. Briet M, Boutouyrie P, Laurent S, London GM. Arterial stiffness and pulse pressure in CKD and ESRD. *Kidney Int*. 2012;82:388–400. <https://doi.org/10.1038/ki.2012.131>.
 60. Fortier C, Mac-Way F, Desmeules S, Marquis K, De Serres SA, Lebel M, Boutouyrie P, Agharazii M. Aortic-brachial stiffness mismatch and mortality in dialysis population. *Hypertension*. 2015;65:378–84. <https://doi.org/10.1161/hypertensionaha.114.04587>.
 61. Stone K, Fryer S, Meyer ML, Kucharska-Newton A, Faulkner J, Zieff G, Paterson C, Credeur D, Matsushita K, Hughes T, Tanaka H, Stoner L. The aortic-femoral arterial stiffness gradient: an atherosclerosis risk in communities (ARIC) study. *J Hypertens*. 2021;39(7):1370–7. <https://doi.org/10.1097/HJH.0000000000002808>.
 62. Bao W, Wang F, Tang W. Aortic-brachial stiffness mismatch and mortality in peritoneal dialysis patients. *Kidney Blood Press Res*. 2019;44:123–32. <https://doi.org/10.1159/000498876>.
 63. Covic A, Siritopol D. Pulse wave velocity ratio: the new “gold standard” for measuring arterial stiffness. *Hypertension*. 2015;65:289–90. <https://doi.org/10.1161/hypertensionaha.114.04678>.
 64. Parker KH, Alastruey J, Stan GB. Arterial reservoir-excess pressure and ventricular work. *Med Biol Eng Comput*. 2012;50:419–24. <https://doi.org/10.1007/s11517-012-0872-1>.
 65. Parker KH. Arterial reservoir pressure, subservient to the McDonald lecture, *Artery* 13. *Artery Res*. 2013;7(3–4):171–85. <https://doi.org/10.1016/j.artres.2013.10.391>.
 66. Parker KH. The reservoir-wave model. *Artery Res*. 2017;18(C):87–101. <https://doi.org/10.1016/j.artres.2017.04.003>.
 67. Segers P, Verdonck P. Role of tapering in aortic wave reflection: hydraulic and mathematical model study. *J Biomech*. 2000;33:299–306. [https://doi.org/10.1016/S0021-9290\(99\)00180-3](https://doi.org/10.1016/S0021-9290(99)00180-3).
 68. Nichols WW, Conti CR, Walker WE, Milnor WR. Input impedance of the systemic circulation in man. *Circ Res*. 1977;40:451–8. <https://doi.org/10.1161/01.res.40.5.451>.
 69. Noble M. Left ventricular load, arterial impedance and their interrelationships. *Cardiovasc Res*. 1979;13:183–98.

70. O'Rourke MF. Vascular impedance in studies of arterial and cardiac function. *Physiol Rev.* 1982;62:570–623. <https://doi.org/10.1152/physrev.1982.62.2.570>.
71. Dintenfass L. Internal viscosity of the red cell and a blood viscosity equation. *Nature.* 1968;219(5157):956–8. <https://doi.org/10.1038/219956a0>.
72. Li JK, Melbin J, Riffle RA, Noordergraaf A. Pulse wave propagation. *Circ Res.* 1981;49:442–52. <https://doi.org/10.1161/01.res.49.2.442>.
73. Dintenfass L. Inversion of the Fahraeus-Lindqvist phenomenon in blood flow through capillaries of diminishing radius. *Nature.* 1967;215:1099–100. <https://doi.org/10.1038/2151099a0>.
74. Chebbi R. Dynamics of blood flow: modeling of the Fähræus-Lindqvist effect. *J Biol Phys.* 2015;41:313–26. <https://doi.org/10.1007/s10867-015-9376-1>.
75. Ince C. The elusive microcirculation. *Intensive Care Med.* 2008;34:1755–6. <https://doi.org/10.1007/s00134-008-1131-7>.
76. Avolio AP. Multi-branched model of the human arterial system. *Med Biol Eng Comput.* 1980;18:709–18. <https://doi.org/10.1007/BF02441895>.

Ready to submit your research? Choose BMC and benefit from:

- fast, convenient online submission
- thorough peer review by experienced researchers in your field
- rapid publication on acceptance
- support for research data, including large and complex data types
- gold Open Access which fosters wider collaboration and increased citations
- maximum visibility for your research: over 100M website views per year

At BMC, research is always in progress.

Learn more biomedcentral.com/submissions

